

UNIVERSITÀ DEGLI STUDI DI NAPOLI “FEDERICO II”



TESI DI DOTTORATO DI RICERCA IN INGEGNERIA ELETTRICA
(XVIII Ciclo)

**ACTIVE POWER FILTERS: BEHAVIOUR AND
PERFORMANCE ANALYSIS**

Tutore:
prof. ing. Enrico Pagano

Addottorando:
dott. ing. Pietro Tricoli

Coordinatore del Dottorato:
prof. ing. Giovanni Miano

NAPLES, 28TH NOVEMBER 2005

INDEX OF CONTENTS

INTRODUCTION	p. 1
I. TOPOLOGIES OF ACTIVE POWER FILTERS	
I.1. INTRODUCTION	p. 5
I.2. TYPES OF HARMONIC SOURCES	p. 9
I.3. CHARACTERISTIC ANALYSIS OF SHUNT ACTIVE FILTERS	p. 11
<i>I.3.a. Compensation analysis for harmonic current sources</i>	p. 13
<i>I.3.b. Compensation analysis for harmonic voltage sources</i>	p. 16
I.4. CHARACTERISTIC ANALYSIS OF SERIES ACTIVE FILTERS	p. 18
<i>I.4.a. Compensation analysis for harmonic current sources</i>	p. 19
<i>I.4.b. Compensation analysis for harmonic voltage sources</i>	p. 21
I.5. COMPARISON OF PARALLEL ACTIVE FILTERS AND SERIES ACTIVE FILTERS	p. 22
I.6. CONCLUSIONS	p. 23
II. SHUNT ACTIVE FILTERS CONNECTED TO THREE PHASE NETWORKS	
II.1. INTRODUCTION	p. 25
II.2. MATHEMATICAL MODEL OF SHUNT ACTIVE FILTERS	p. 26
II.3. ACTIVE FILTER CONNECTED TO THE NETWORK WITHOUT INDUCTANCES	p. 29
<i>II.3.a. Square-wave inverters</i>	p. 31
<i>II.3.b. Numerical results of inverter driven by square-wave control</i>	p. 35
II.4. ACTIVE FILTER WITH INDUCTANCES DRIVEN WITH SQUARE-WAVE CONTROL	p. 39
<i>II.4.a. The modified z-transform method</i>	p. 40
<i>II.4.b. The application of the modified z-transform to active filters</i>	p. 42
<i>II.4.c. Numerical results</i>	p. 52
<i>II.4.d. Harmonic analysis</i>	p. 56
II.5. CONCLUSIONS	p. 58

III. DIMENSIONING PROCEDURE OF THE PASSIVE ELEMENTS OF AN ACTIVE FILTER

III.1. INTRODUCTION	p. 59
III.2. APPLICATION TO THE DESIGN GUIDELINES	p. 61
III.3. SAMPLE DIMENSIONING WITH NUMERICAL VERIFICATION	p. 64
III.4. COST OPTIMIZATION FOR THE INDUCTIVE FILTER DESIGN	p. 66
III.5. CONCLUSIONS	p. 71

IV. CONTROL TECHNIQUES OF ACTIVE FILTERS USED FOR HARMONIC COMPENSATION

IV.1. INTRODUCTION	p. 75
IV.2. FEEDING ALGORITHM USED FOR HARMONIC COMPENSATION	p. 77
<i>IV.2.a. Feeding algorithm used for harmonic compensation</i>	p. 80
<i>IV.2.b. Feeding algorithm used for load balancing</i>	p. 83
IV.3. NUMERICAL RESULTS	p. 84
IV.4. CONCLUSIONS	p. 88

V. VALIDATION OF THE MATHEMATICAL MODEL: EXPERIMENTAL RESULTS

V.1. THE TEST BENCH	p. 91
V.2. EXPERIMENTAL RESULTS WITHOUT INDUCTANCES	p. 92
V.3. EXPERIMENTAL RESULTS WITH INDUCTANCES	p. 102
V.4. CONCLUSIONS	p. 104

REFERENCES	p. 111
-------------------	--------

INTRODUCTION

Power electronics devices are widely used in different fields and for different practical applications. The expansion of their field of applications is related to the knowledge of the device behaviour and of their performances. One of the most interesting field of application is load compensation, i.e. active filtering of load harmonics, load unbalance and / or load power factor compensation. Both items require a proper drive of power electronics apparatus. This result can be easily obtained by designing specific software programmes. The development of these programmes can be satisfactorily made only on the basis of the theoretical knowledge and of the preliminary evaluation of mathematical models of power electronics devices. It is well-known that these devices make largely use of solid-state semiconductor switches. They have non-linear electric characteristics that lead to complicate analytical expressions of mathematical models. An important step for solving many practical problems are researches devoted to evaluate solutions of non linear system of differential equations that depict mathematical models of such devices. It is indeed not easy to get general solutions of these problems but it can be considered a remarkable research effort to try to find solutions for specific devices. In order to obtain these results, integral transformations are sometimes useful, because operations in complex domains make it possible to find easier solutions in analytical closed form.

The approach to the analysis of behaviour of active filters has been carried out by means of a mathematical procedure based on the modified z -transform method. The solution, suitable both during transients and at steady state, is expressed by means of well-known mathematical functions. This solution can be very useful in practice because it leads not only to understand easily the filter behaviour and the influence of inner parameter values, but also it gives guidelines for the design of passive elements and for the implementation of suitable control algorithms.

Both compensations must obviously be performed with reference to instantaneous values of main electrical quantities and in particular to instantaneous values of the power factor, reactive power and harmonics. Actually, all these quantities are traditionally referred to electrical quantities represented by sinusoidal functions or, in an extended way, almost by periodical functions. The evaluation of software for active filtering operations can be easily carried out on the basis of proper definitions of new compensating criteria. These are evaluated by extending the traditional definitions (referred to a waveform period) to proper instantaneous quantities. Technical literature has widely examined the problem and useful practical solutions have been suggested. Most active power filters are controlled on the basis of instantaneous reactive power theory, also known as Akagi and Nabae theory. The line currents are forced to be sinusoidal if the active filter is capable of holding constant the instantaneous active power. In addition, the reactive power compensation is achieved if the active filter is also capable of holding constant and nil the instantaneous imaginary power. The instantaneous imaginary power, which is a theoretical quantity without physical meaning, is an extension of the reactive power definition to instantaneous values.

However, the analysis of technical literature has pointed out that the results obtained are not fully suitable for the evaluation of the active filter control techniques which actually obtain the compensation of a given harmonic set. This problem can be solved only on the basis of the knowledge of the analytical relationships between harmonics generated by the filter and its control laws. On the basis of the theoretical study made on the active filter mathematical model, a feeding algorithm for compensating a given harmonic current set and the reactive power has

been designed. The algorithm is valid in general, even if unsymmetrical voltages and unbalanced currents are involved. The output of the feeding algorithm is the reference signal for the Space Vector Modulation of the inverter voltage, which actually allows the obtainment of the desired load compensation.

In order to verify the correctness and the accuracy of theoretical results, the mathematical model proposed and the analytical procedure followed have been finally validated by experimental tests carried out on a sample shunt active filter connected to the power network.

I

TOPOLOGIES OF ACTIVE POWER FILTERS

I.1. INTRODUCTION

Interference due to harmonics, and generated by power electronic devices, has become a serious problem, because converters are nowadays more and more frequently used in industrial applications, in transmission and distribution systems and in power plants. The most natural, suitable way to solve these problems is the introduction of filtering actions. Passive LC filters have long been used to absorb harmonic current of non-linear loads. Their advantages are principally low cost and high efficiency. However, passive filters have also some disadvantages, which have been already evidenced in the technical literature. First of all, the mistuning due to component tolerances of inductors and capacitors affects negatively filtering characteristics modifying cut-off frequencies and phase delays. Moreover, the passive filter acts as a sink to the harmonics of the source voltage, because it presents an impedance at specific harmonic frequencies lower than that of the load impedance. Finally, the compensation characteristics of passive filters are influenced by the source impedance, which is not usually known accurately and depends on the instantaneous configuration of the power network.

The development of the technology allowed the introduction of new devices able to satisfy the constraints previously explained. These new devices realise a static conversion of electrical energy and they make use of solid state semi-conductors. The increase of their reliability in the last years has allowed their diffusion on the large scale in different application fields. Significant examples are the conversion substations with rectifiers for transmission lines with dc current outputs and the electrical drives which obtain flexible outputs with variable voltages and frequencies. The basic working principle of solid-state electronic devices is however strongly different from that of equipment realised with rotating machines. The semi-conductors inside static converters are indeed devices with a strongly non linear behaviour and, when they are introduced in electrical networks, they produce a considerable distortion of voltages and currents. In more correct words, the use of semiconductors involves the presence of current harmonics over the fundamental, which is respectively the mean value of the waveform for dc current systems and the harmonic having the frequency equal to the inverse of the period of the waveform for ac current systems. Static converters need also reactive power for operating and such a power has to be supplied by the mains. The harmonic currents flowing into the mains cause also greater losses on the transmission line and distortions of supplying voltages, that cause problems for the other loads connected to the mains.

Since the basic compensation principles of active filters were proposed around 1970 [1, 2, 3, 4, 5, 6], they have been studied by many researchers and engineers aiming to put them into practical applications. Shunt active filters for harmonic compensation, with or without reactive power compensation, flicker compensation or voltage regulation have been put on a commercial base, and their ratings have ranged from 50 kVA to 60 MVA at present. In the next future, it is expected that active filters will cover fields of application much wider than those covered in 1970. The use of active filters will be expanded from the voltage flicker compensation or voltage regulation into the power quality improvement for power distribution systems, as the ratings of active filters increase.

A number of low-power electronic-based appliances such as TV sets, personal computers, and adjustable speed heat pumps generate a large amount of harmonic current in power systems even though a single low-power electronic-based appliance, in which a single-phase diode rectifier with a dc link capacitor is used as utility interface, produces a negligible amount of harmonic current. Three-phase diode or thyristor rectifiers and cycloconverters for industry applications also generate a large amount of harmonic current.

The voltage distortion resulting from current harmonics produced by power electronic equipment, has become a serious problem to be solved in many countries. The guidelines for harmonic mitigation are currently applied on a voluntary basis to keep harmonic levels monitored and promote better practices in both power systems and equipment design. In general, individual low-power end-users and high-power consumers are responsible for limiting the current harmonics caused by power electronic equipments, while electric power companies are responsible for limiting voltage harmonics at the point of common coupling (PCC) in power transmission and distribution systems. The advance of power electronics technology over the last ten years, along with the theory of instantaneous active and reactive power in three-phase circuits, presented in 1983 [7], has made it possible to put active filters into practical applications, not only for harmonic compensation with or without reactive power compensation [8, 9], but also for flicker compensation [10] and regulation of voltage drop at the end terminal of a power system. All the active filters installed have been placed by individual high-power consumers on their own premises near the loads producing harmonics. The shunt active filters have presented filtering characteristics much more satisfactory than conventional shunt passive filters and/or static VAr compensators based on thyristor-controlled reactors.

Traditional harmonic sources have been mainly the phase-controlled thyristor rectifiers and cycloconverters, which can be regarded as current-source loads. On the other hand, since more and more diode rectifiers with smoothing dc capacitors are used in electronic equipment, household appliances, and ac drives, harmonics generated by these loads have become a major issue. Naturally, attempts have been made to use shunt active filters for harmonic compensation of these diode rectifiers. However, it has been found in the practical application that the parallel active filters not only cannot cancel the harmonics completely but also cause problems, such as enlarging the dc volt-age ripples and ac peak current of the rectifier. This is because a diode rectifier with smoothing dc capacitors behaves like a harmonic voltage source rather than as a harmonic current source.

This chapter highlight the application issues of both shunt and series active filters in power systems. Their features and required operation conditions are clarified analytically and compared one to the others.

I.2. TYPES OF HARMONIC SOURCES

As it is well-known, thyristor converters are a common source of harmonic currents. The distortion of the current, i.e. the presence of harmonics in the Fourier expansion of the waveform, results from the switching operation of thyristors. Fig.1.1a shows a typical thyristor rectifier, where a large choke in the dc link produces a current almost constant. Fig.1.2 shows also the load voltage and the source current waveforms supplied to the rectifier. Since the harmonic current contents and the characteristics are not dependent on the ac side, this type of harmonic source behaves like a current source. Therefore, they are called current-source type of harmonic source (or harmonic current source) and represented as a current source, as shown in Fig.1.1b.

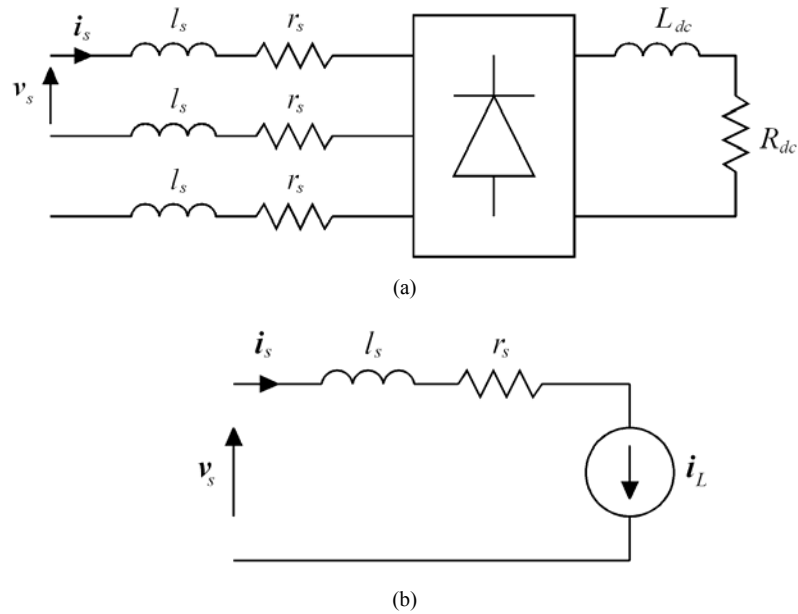


Fig.1.1. Typical harmonic current source (a) and its equivalent electrical circuit (b)

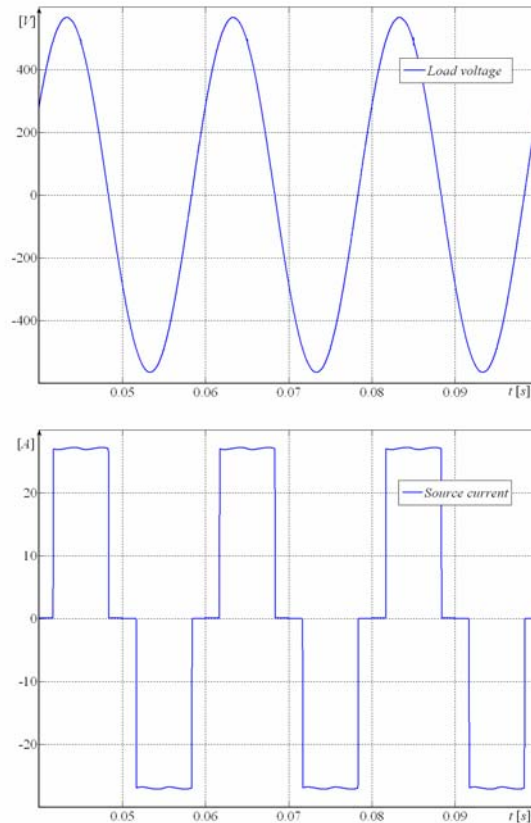


Fig.1.2. Typical current and voltage waveforms of a diode rectifier with large dc inductor

Nowadays, another common harmonic source is that of diode rectifiers with smoothing dc capacitors, as shown in Fig.1.3a. Fig.1.4 shows the current and voltage waveforms of steady-state operations of such a rectifier. Although the current is highly distorted, its harmonic amplitude is greatly affected by the impedance of the ac side, whereas the rectifier voltage (i.e. the voltage across the rectifier input terminal as shown in Fig.1.4) is not dependent on ac impedance. Therefore, a diode rectifier behaves like a voltage source rather than a current source. Fig.1.3b shows the equivalent circuit of the diode rectifier system, where the diode rectifier is represented by a voltage-source type of harmonic source (or harmonic voltage source). Accordingly, the harmonic currents flowing into the ac line and generated by the rectifier voltage are dependent on the rectifier voltage and the ac impedance.

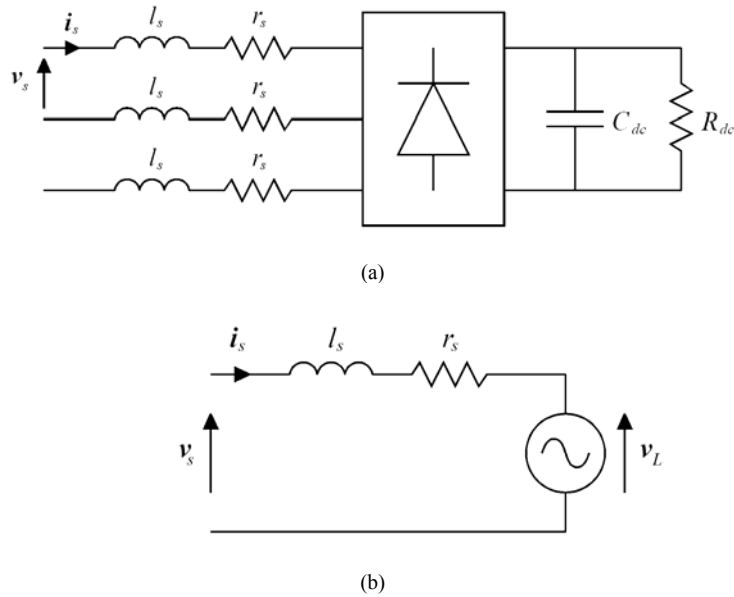


Fig.1.3. Typical harmonic voltage source (a) and its equivalent electrical circuit (b)

I.3. CHARACTERISTIC ANALYSIS OF SHUNT ACTIVE FILTERS

A shunt active filter is an inverter driven by a pulse-width modulation technique (PWM) and placed in parallel with a load (or a harmonic source), as fig.1.5 shows. The shunt active filter injects a harmonic currents with the same amplitude of those of the load into the ac system but with opposite phase displacement.

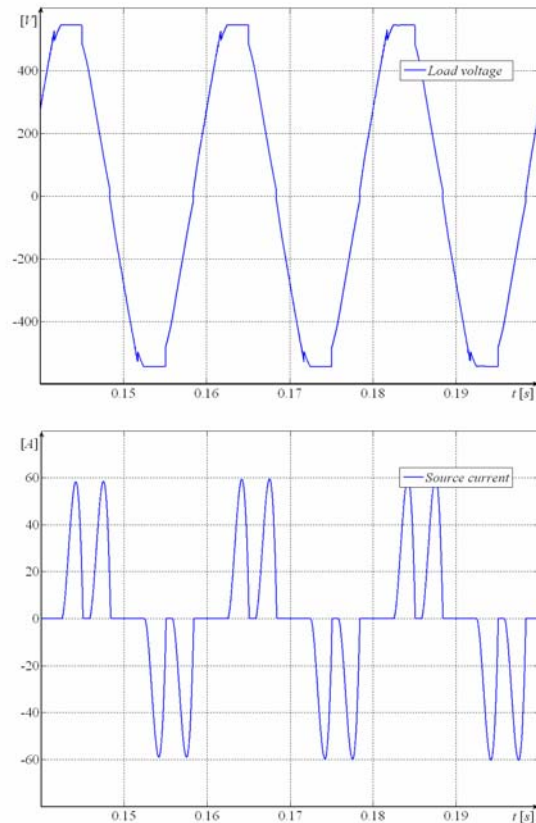


Fig.1.4. Typical voltage and current waveforms of a diode rectifier with large dc capacitor

The filter control is implemented through a detection and extraction circuit of the load harmonic currents. At steady-state, ideally, the compensating current can be supposed to be dependent on the load current by means of a proper transfer function, representing the selected control technique of active filter. With this simplification the analysis of

the compensation characteristics of filters is straightforward, if reference is made to the equivalent circuits at the different harmonics. The

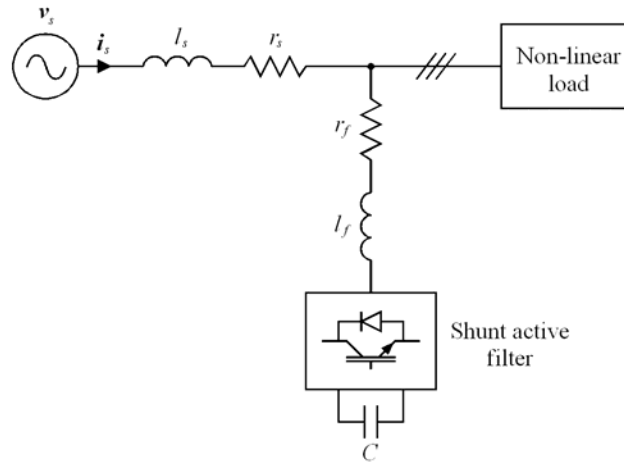


Fig.1.5. Configuration of a shunt active filter system

harmonic current sources can be, hence, respectively represented by their Norton equivalent circuit, and the harmonic voltage sources by their Thevenin equivalent circuit, as Figs.1.6 and 1.7 show. A pure current-source type of harmonic source is a special case of the Norton equivalent circuit when $Z_L \rightarrow \infty$. A pure voltage-source type of harmonic source is a special case of Thevenin equivalent circuit when $Z_L \rightarrow 0$. In the following, the compensation characteristics of a shunt active filter are considered in the both cases of harmonic current sources and harmonic voltage sources.

1.3.a. Analysis of compensation for harmonic current sources

Fig.1.6 shows the basic principle of a parallel active filter compensating for a harmonic current source, which is represented by its Norton equivalent circuit.

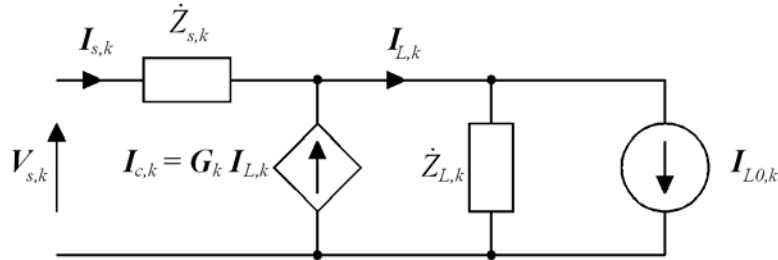


Fig.1.6. Equivalent network of a shunt active filter for harmonic current source

In Fig.1.6, $Z_{s,k}$ is the source impedance, $I_{L,0,k}$ is the equivalent harmonic current source, $Z_{L,k}$ is the equivalent impedance on the load side, which may include passive filters and power-factor correction capacitors, and G_k is the equivalent transfer function of the active filter including the detection circuit of harmonics and the delay of the control circuit. Generally, G_k has to notch the component at the fundamental frequency, i.e. $G_1 = 0$, and to let to flow the harmonic components, i.e. $G_k = 1, k > 1$. From Fig.1.5, the following equations are obtained:

$$I_{c,k} = G_k I_{L,k} ; \quad (1.1)$$

$$I_{s,k} = \frac{Z_{L,k}}{Z_{s,k} + \frac{Z_{L,k}}{1 - G_k}} I_{L,0,k} + \frac{1}{Z_{s,k} + \frac{Z_{L,k}}{1 - G_k}} V_{s,k} ; \quad (1.2)$$

$$I_{L,k} = \frac{\frac{Z_{L,k}}{1-G_k}}{Z_{s,k} + \frac{Z_{L,k}}{1-G_k}} I_{L0,k} + \frac{\frac{1}{1-G_k}}{Z_{s,k} + \frac{Z_{L,k}}{1-G_k}} V_{s,k}. \quad (1.3)$$

Focusing on harmonics, when the following equation:

$$\frac{Z_{L,k}}{|1-G_k|} \gg Z_{s,k} \quad (1.4)$$

is satisfied, (1.1), (1.2) and (1.3) can be rewritten as:

$$I_{c,k} = I_{L,k}; \quad (1.5)$$

$$I_{s,k} = (1-G_k)I_{L0,k} + \frac{(1-G_k)}{Z_{L,k}} V_{s,k}; \quad (1.6)$$

$$I_{L,k} = I_{L0,k} + \frac{V_{s,k}}{Z_{L,k}}. \quad (1.7)$$

Eq. (1.6) shows that the source current becomes sinusoidal because of $|1-G_k| \cong 0$ for each harmonic when (1.4) is satisfied. Therefore, (1.4) is the required operating condition for the parallel active filter to cancel the load harmonic current. From (1.4), it can be seen that only G_k can be pre-designed and determined by the active filter, whereas $Z_{s,k}$ and $Z_{L,k}$ are determined by the system, i.e., the ac source impedance and the load characteristics. Therefore, the compensation characteristics of the active filter are determined not only by the active filter itself but also by the ac source and load impedance, like conventional passive filters.

Equation (1.6) shows that compensation characteristics of the active filter are not influenced by the source impedance, $Z_{s,k}$. Although this is true only under the condition (1.4) this property makes active filters better than passive filters. Equation (1.4) can be easily satisfied by active filters, since G_k is determined by the filter control technique, and mainly dominated by the detection circuit of harmonics, the delay time of the control circuit, and the current response of the inverter.

However, when a shunt passive filter or power-factor improvement capacitor bank is connected on the side of the thyristor rectifier, the load impedance is very small also for harmonics. Consequently, the compensation characteristics of the active filter are influenced by the source impedance, because the condition (1.4) is no longer satisfied. Moreover, it is clear that the current flowing into the passive filter connected to the load side is given by eq. (1.7). This current may be extraordinarily large when the ac source is stiff and has appreciable voltage harmonic distortion, $V_{s,k}$. This means that ambient harmonics upstream will flow into the passive filter. The load harmonic current, $I_{L0,k}$, are entirely compensated by the active filter but not by the passive filter and this one instead absorbs all ambient harmonics upstream. Therefore, special considerations are needed when a parallel passive filter and a shunt active filter are placed in the same power system. If a combined system of shunt active filter and shunt passive filter is used for compensating load harmonics, the compensation responsibility of both the active filter and the passive filter should be clear and well controlled. For example, the use of an active filter to compensate for the fifth and seventh order harmonics and a passive filter for higher order harmonics is a good responsibility-sharing of harmonic compensation, because an active filter is better for lower order harmonic compensation and a passive filter is better for higher order harmonic compensation. In this case, only the fifth and seventh order harmonics of the load current should be extracted as the reference of the active filter so that the active filter would not inject higher order

harmonic current into the line.

1.3.b. Analysis of compensation for harmonic voltage sources

Fig.1.7 shows the basic principle of shunt active filter compensating for a harmonic voltage source, where the load is represented as Thevenin equivalent, i.e., a voltage source $V_{L0,k}$ with an impedance $Z_{L,k}$. From Fig.1.7, the following equations can be written:

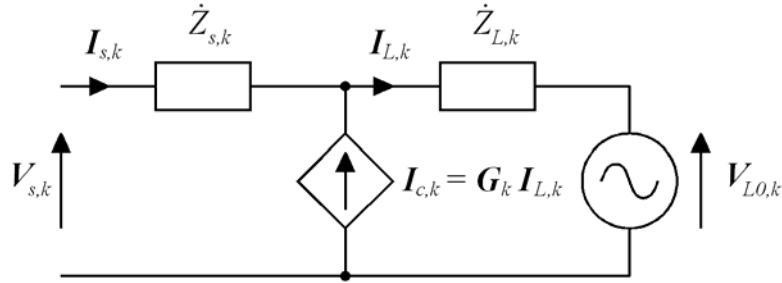


Fig.1.7. Equivalent network of a shunt active filter for harmonic voltage source

$$I_{s,k} = \frac{V_{s,k} - V_{L0,k}}{Z_{s,k} + \frac{Z_{L,k}}{1 - G_k}}, \quad (1.8)$$

$$I_{L,k} = \frac{1}{1 - G_k} \frac{V_{s,k} - V_{L0,k}}{Z_{s,k} + \frac{Z_{L,k}}{1 - G_k}} = \frac{V_{s,k} - V_{L0,k}}{Z_{s,k}(1 - G_k) + Z_{L,k}}. \quad (1.9)$$

Therefore, when the following equation:

$$Z_{L,k} \gg Z_{s,k} |1 - G_k| \quad (1.10)$$

is satisfied, the source current will become sinusoidal, i.e.:

$$I_{c,k} = I_{L,k}, \quad (1.11)$$

$$I_{s,k} \cong 0, \quad (1.12)$$

$$I_{L,k} = \frac{V_{s,k} - V_{L0,k}}{Z_{L,k}}. \quad (1.13)$$

Eq. (1.10) is the required operating condition that should be satisfied when a shunt active filter compensates for a harmonic voltage source. However, eq. (1.10) cannot be easily satisfied by a shunt active filter, because a harmonic voltage source usually presents a very low internal impedance. For example, considering a diode rectifier with a large smoothing electrolytic dc capacitor, there results $Z_{L,k} \cong 0$ as long as no series reactor is placed on the ac side of the rectifier. Therefore (1.11) cannot be satisfied only with the source impedance, which is usually under 10% (0.1 pu).

Moreover, it is evident from eqs. (1.9), (1.11) and (1.13) that:

- the shunt active filter makes the source impedance equivalent to zero, as seen from the load side, thus lowering ac impedance to the load;
- the harmonic currents injected by the filter flow into the load;
- the distortion of the source voltage, $V_{s,k}$, also causes a large harmonic current flowing into the load.

These effects largely increase the load harmonic currents and the required volt-ampere rating of the shunt active filter, especially when Z_L is small.

I.4. CHARACTERISTIC ANALYSIS OF SERIES ACTIVE FILTERS

As discussed in this chapter and fig.1.8 shows, a series active filter has to be placed in series between the ac source and the load in order to force the source current to become sinusoidal. The approach is based on a principle of harmonic isolation by controlling the output voltage of the series active filter. In other words, the series active filter has to present high impedance to harmonic currents and then it is able to block these currents from the load to the ac source and from the ac source to the load.

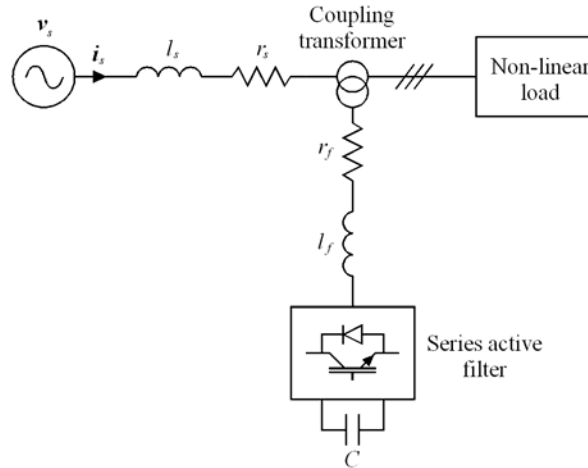


Fig.1.8. Configuration of a series active filter system

As in the previous section, the characteristics of series active filters are analysed for both harmonic current sources and harmonic voltage sources.

I.4.a. Analysis of compensation for harmonic current sources

Fig.1.9 shows the basic principle of a series active filter compensating for a harmonic current source, where $V_{c,k}$ represents the output voltage of the filter and the load is represented by its Norton equivalent circuit. If the series active filter control technique is:

$$V_{c,k} = H_k I_{L,k} \quad (1.14)$$

then the source current is as follows:

$$I_{s,k} = \frac{Z_{L,k}}{Z_{s,k} + Z_{L,k} + H_k} I_{L0,k} + \frac{I}{Z_{s,k} + Z_{L,k} + H_k} V_{s,k}, \quad (1.15)$$

where H_k is the equivalent transfer function of a detection circuit of harmonic current, including delay time of the control circuit. H_k is

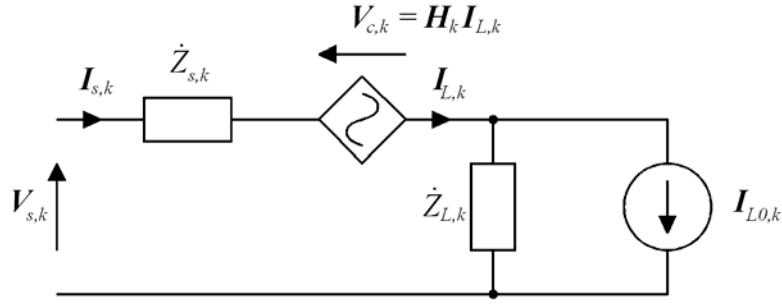


Fig.1.9. Equivalent network of a series active filter for harmonic current source

supposed equal to zero at the fundamental and approximately equal to 1 for harmonics, i.e. $H_1 = 0$ and $H_k = 1$, for $k > 1$. The function H has the dimension of ohms in pu. The distortion voltage of the ac source, $V_{s,k}$, usually causes current harmonics much smaller than those produced by the harmonic source. Therefore when the conditions:

$$H_k \gg \left| \mathcal{Z}_{s,k} + \mathcal{Z}_{L,k} \right| \quad (1.16)$$

are satisfied, there results:

$$V_{c,k} \cong \mathcal{Z}_{L,k} I_{L0,k} + V_{s,k} \quad (1.17)$$

$$I_{s,k} \cong 0 \quad (1.18)$$

and then the source current becomes sinusoidal. The eqs. (1.16) are the required operating conditions for the series active filter to compensate harmonic current sources. Eq. (1.16) requires that the H_k should be large and the impedance of the load side, $Z_{L,k}$, be small for harmonics in order to suppress the source harmonic current. However, for a conventional phase-controlled thyristor rectifier, Z_L is very large, so that eq. (1.17) cannot be easily satisfied.

It is clear from (1.17) that the required output voltage of the series active filter, $V_{c,k}$, also becomes infinite. As a result, the series active filter cannot compensate for a current-source type of harmonic source theoretically. If a shunt passive filter is placed with the thyristor rectifier $Z_{L,k}$ becomes conversely very small, eq. (1.17) can be satisfied without problems and the required output voltage, $V_{c,k}$, becomes very small as well. This means that a combined system of series active filter and parallel passive filter is a solution suitable also for compensating current-source type of harmonic source. In addition, it should be noted that the series active filter has a very important feature because it provides harmonic isolation between the source and load. Eqs. (1.17) and (1.18) indicate that neither the source harmonics, $V_{s,k}$, appears on the load side, nor the load harmonics, $I_{L0,k}$, flows into the ac source.

1.4.b. Analysis of compensation for harmonic voltage sources

Fig.1.10 shows the basic principle of series active filter compensating for a harmonic voltage source. If the series active filter is controlled as:

$$V_{c,k} = H_k I_{L,k} \quad (1.19)$$

the source current becomes:

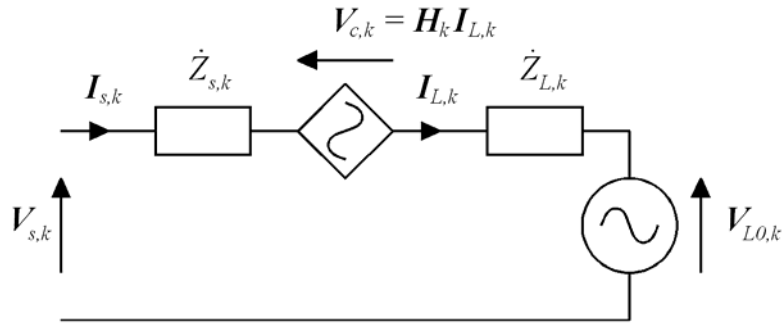


Fig.1.10. Equivalent network of a series active filter for harmonic voltage source

$$I_{s,k} = \frac{V_{s,k} - V_{L0,k}}{\underline{Z}_{s,k} + \underline{Z}_{L,k} + H_k} \quad (1.20)$$

Therefore, when:

$$H_k \gg |\underline{Z}_{s,k} + \underline{Z}_{L,k}| \quad (1.21)$$

there results:

$$V_{c,k} \cong V_{s,k} - V_{L0,k} \quad (1.22)$$

$$I_{s,k} \cong 0 \quad (1.23)$$

The condition (1.21) is the required operating condition for the series active filter to compensate for a harmonic voltage source load, which depends only on the series active filter itself. It is also clear from (1.23) that the compensation characteristics of the series active filter are independent on the source impedance Z_s and the load impedance Z_L . Therefore the series active filter can suppress harmonics of the source current effectively. These conclusions regarding the series active filter compensating for a harmonic voltage-source load are completely equivalent to those of the parallel active filter compensating for a harmonic current-source load.

I.5. COMPARISON OF PARALLEL ACTIVE FILTERS AND SERIES ACTIVE FILTERS

In the previous sections, compensation characteristics of shunt active filters and series active filters have been analysed theoretically. The corresponding required operating conditions of both shunt active filter and series active filter for harmonic current sources and harmonic voltage sources, respectively, have been derived. In circuit configurations, duality relationships exist between shunt active filters and series active filters, i.e. Fig.1.6 is the dual of Fig.1.10, and Fig.1.7 is the dual of Fig.1.8. Therefore, the properties of the corresponding harmonic sources are each the dual of the other. Tab.1.I summarises a comparisons of shunt active filters and series active filters, where their respective features and application considerations are listed.

I.6. CONCLUSIONS

Common non-linear loads have been characterised into two types of harmonic sources, current-source type of harmonic source and voltage-source type of harmonic source. Compensation characteristics of both shunt active filters and series active filters have been discussed for these two types of harmonic sources. The corresponding required operation conditions, features and application issues of both filters have been presented. Shunt active filters have very good compensation characteristics for harmonic current sources, but they may increase harmonic currents and may cause overcurrent when the load is a harmonic voltage source. Instead, series active filters are more

suitable for compensation of a harmonic voltage source such as a diode rectifier with smoothing dc capacitor. Finally a comparison between shunt and series active filters has been made in order to show the advantages and disadvantages of their use with different loads and in different operating conditions.

Tab.1.1 – Comparison of shunt active filters and series active filters

System Configuration	Shunt AF	Series AF
Basic Operation Principle	Operates as a current source	Operates as a voltage source
Adaptive loads	Inductive or harmonic current-source loads, e.g. phase controlled thyristor rectifiers for dc drives	Capacitive or voltage source loads, e.g. diode rectifiers with direct smoothing capacitors for ac drives
Required operation conditions	The load impedance should be high	The load impedance should be low
Compensation characteristics	Excellent and independent on the source impedance for current-source loads, but depends on the source impedance when the load impedance is low	Excellent and independent on the source impedance and of the load impedance for voltage-source loads, but depends on the source impedance when the load is current-source type
Application consideration	Injected current flows into the load side and may cause overcurrent when applied to a capacitive or voltage source load	A load impedance parallel branch (parallel passive filter or power factor improvement capacitor bank) is needed when applied to an inductive or current source load

II

SHUNT ACTIVE FILTERS CONNECTED TO THREE PHASE NETWORKS

II.1. INTRODUCTION

The analysis of the behaviour of an active filter can be successfully performed by using the results of the study of its mathematical model. In this chapter the mathematical model of a shunt active filter connected to a three phase network is determined. The approach to the analysis of behaviour of active filters has been carried out by means of a simple mathematical procedure, which can be used only if filter inductances are neglected. The achieved results have been very useful for defining the sensitivity of the filter behaviour to its parameter variations within large ranges. This simple mathematical procedure cannot be, however, successfully applied to a real filter structure, where inductances obviously play an important role. Therefore, the method of the modified z -transform has been used and it has been verified that the procedure leads to obtain an analytical solution of the non-linear mathematical model of active filters. The solution is written in a closed form and expressed by means of well-known mathematical functions. This can be very useful in practice because it leads not only to understand easily the filter behaviour and the influence of inner parameter values, but also gives guidelines for the design of passive elements and the implementation of suitable control algorithms.

The solving procedure consists of two following steps. The first one is devoted to processing a traditional mathematical model of active filters until it gives a final system of non-linear differential equations expressed by means of Dirac Delta functions. The last step applies the modified z -transform technique to solve equations and to obtain final analytical solutions. Due to the formal complexity of the mathematical model it would be a nonsense to expect to obtain simple expressions of final solutions. These are, however, given by well-known functions, which easily allow the researchers the analysis of filter behaviour and the influence of filter parameter variation. The mathematical procedure makes it possible to obtain a closed-form solution both during transients and at steady state and then to evaluate harmonic filtering capability and reactive power compensation.

II.2. MATHEMATICAL MODEL OF SHUNT ACTIVE FILTERS

For sake of simplicity reference has been made to the ideal filter configuration represented by the equivalent electrical network of fig.2.1. The filter is connected to an infinite power network and operates like a shunt active filter. Therefore, the circuit configuration of fig.2.1 leads to write the following system of non-linear differential equations. This is the mathematical model of the physical system represented by the sample filter structure taken into consideration:

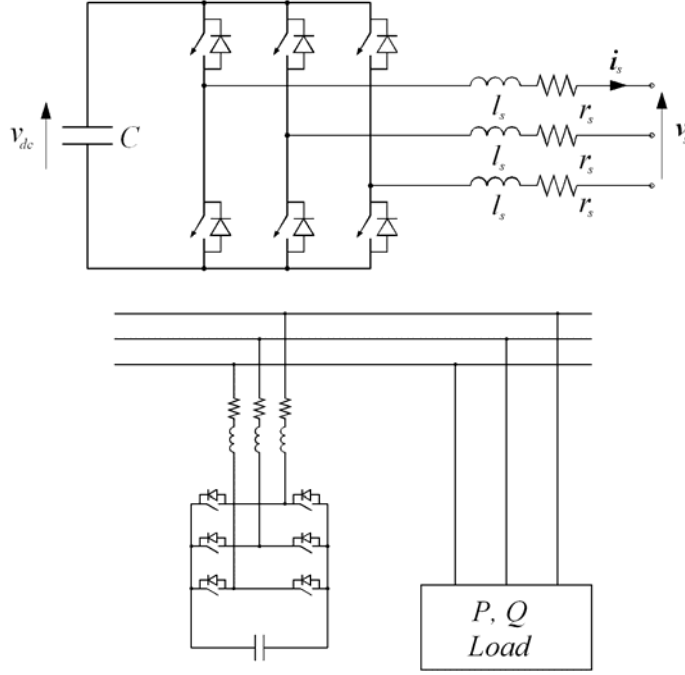


Fig.2.1. Equivalent electrical networks of a sample configuration of a shunt active filter

$$\begin{cases} \mathbf{v}_s + r_s \mathbf{i}_s + l_s \frac{d\mathbf{i}_s}{dt} = \frac{2}{3} v_{dc} \boldsymbol{\zeta}(t) e^{j\frac{\pi}{3}\eta(t)} ; \\ \frac{dv_{dc}}{dt} = -\frac{1}{C} \text{Re} \left\{ \mathbf{i}_s \boldsymbol{\zeta}(t) e^{-j\frac{\pi}{3}\eta(t)} \right\}. \end{cases} \quad (2.1)$$

The complex functions \mathbf{v}_s , \mathbf{i}_s are defined in the complex dominion $\{\mathcal{R}e, j \mathcal{I}m\}$. According to the traditional linear combination of time functions, they are equal to:

$$\mathbf{v}_s = \frac{2}{3} \sum_{\rho=0}^2 v_{\rho}(t) e^{j\frac{2\pi}{3}\rho} ;$$

$$\mathbf{i}_s = \frac{2}{3} \sum_{\rho=0}^2 i_{\rho}(t) e^{j\frac{2\pi}{3}\rho} .$$

In eqs. (2.1), $\eta(t)$ and $\zeta(t)$ are integer-valued time functions. The function $\eta(t)$, which assumes values in the range $[0, 5]$, models the phase displacement of the output voltage of the inverter in its six different conduction states. Moreover, the time function $\zeta(t)$ assumes the value 0 when the capacitor is not connected to the network, whereas it assumes the value 1. In practice the function $\zeta(t)$ indicates whether or not the inverter is in one of its active states.

The mathematical model in eqs. (2.1) is valid in general and, as it can be easily seen, it is represented by a system of non-linear differential equations. Multiplying both term of the first equation of system (2.1) by

$\boldsymbol{\zeta}(t) e^{-j\frac{\pi}{3}\eta(t)}$ and putting:

$$\mathbf{v}'_s = \mathbf{v}_s \boldsymbol{\zeta}(t) e^{-j\frac{\pi}{3}\eta(t)} \quad (2.2)$$

$$\mathbf{y} = \mathbf{i}_s \boldsymbol{\zeta}(t) e^{-j\frac{\pi}{3}\eta(t)} \quad (2.3)$$

it is obtained:

$$\begin{cases} \mathbf{v}'_s + r_s \mathbf{y} + l_s \zeta(t) e^{-j\frac{\pi}{3}\eta(t)} \frac{d\mathbf{i}_s}{dt} = \frac{2}{3} v_{dc} \zeta^2(t); \\ \frac{dv_{dc}}{dt} = -\frac{1}{C} \text{Re}\{\mathbf{y}\}. \end{cases}$$

Taking into account that the functions $\zeta(t)$ and $\eta(t)$ can be also discontinuous, the derivative of \mathbf{y} is equal to:

$$\frac{d\mathbf{y}}{dt} = \zeta(t) e^{-j\frac{\pi}{3}\eta(t)} \frac{d\mathbf{i}_s}{dt} + \mathbf{i}_s \left[e^{-j\frac{\pi}{3}\eta(t)} \frac{d\zeta(t)}{dt} + \zeta(t) \frac{d}{dt} e^{-j\frac{\pi}{3}\eta(t)} \right].$$

The rearrangement of the previous equation yields:

$$\zeta(t) e^{-j\frac{\pi}{3}\eta(t)} \frac{d\mathbf{i}_s}{dt} = \frac{d\mathbf{y}}{dt} - \mathbf{y} \left[\frac{1}{\zeta(t)} \frac{d\zeta(t)}{dt} + e^{j\frac{\pi}{3}\eta(t)} \frac{d}{dt} e^{-j\frac{\pi}{3}\eta(t)} \right]$$

and finally:

$$\begin{cases} \mathbf{v}'_s + r_s \mathbf{y} + l_s \frac{d\mathbf{y}}{dt} - l_s \mathbf{y} \left[\frac{1}{\zeta(t)} \frac{d\zeta(t)}{dt} + e^{j\frac{\pi}{3}\eta(t)} \frac{d}{dt} e^{-j\frac{\pi}{3}\eta(t)} \right] = \frac{2}{3} v_{dc} \zeta^2(t); \\ \frac{dv_{dc}}{dt} = -\frac{1}{C} \text{Re}\{\mathbf{y}\}. \end{cases} \quad (2.4)$$

II.3. ACTIVE FILTER CONNECTED TO THE NETWORK WITHOUT INDUCTANCES

The integration of previous system of equations can be analytically carried out only in particular cases. The simplest possibility is to consider that the inverter is connected to the power network only with resistances. Putting $l_s = 0$ in eqs. (2.4) there results:

$$\begin{cases} \mathbf{v}'_s + r_s \mathbf{y} = \frac{2}{3} v_{dc} \zeta^2(t); \\ \frac{dv_{dc}}{dt} = -\frac{1}{C} \text{Re}\{\mathbf{y}\}. \end{cases}$$

Solving the first equation for \mathbf{y} :

$$\begin{cases} \mathbf{y} = -\frac{\mathbf{v}'_s}{r_s} + \frac{2}{3r_s} v_{dc} \zeta^2(t); \\ \frac{dv_{dc}}{dt} = \frac{1}{r_s C} \text{Re}\{\mathbf{v}'_s\} - \frac{2}{3r_s C} v_{dc} \zeta^2(t). \end{cases} \quad (2.5)$$

The second equation of the system (2.5) is a differential equation in the variable v_{dc} , which can be easily solved according to the well-known mathematical theory:

$$\begin{aligned} v_{dc}(t) = e^{-\frac{2}{3r_s C} \int_0^t \zeta^2(x) dx} & \left[v_{dc0} + \right. \\ & \left. + \frac{1}{r_s C} \int_0^t \zeta(\tau) \text{Re}\left\{ \mathbf{v}'_s e^{-j\frac{\pi}{3}\eta(\tau)} \right\} e^{\frac{2}{3r_s C} \int_0^\tau \zeta^2(x) dx} d\tau \right], \end{aligned} \quad (2.6)$$

where $v_{dc0} = v_{dc}(0)$. From the first equation of system (2.5), the expression of the current \mathbf{i}_s can be finally evaluated:

$$\mathbf{i}_s(t) = -\frac{\mathbf{v}_s}{r_s} + \frac{2}{3r_s} \zeta(t) e^{j\frac{\pi}{3}\eta(t) - \frac{2}{3r_s C} \int_0^t \zeta^2(x) dx} \left[\mathbf{v}_{dc0} + \frac{I}{r_s C} \int_0^t \zeta(\tau) \operatorname{Re} \left\{ \mathbf{v}_s e^{-j\frac{\pi}{3}\eta(\tau)} \right\} e^{\frac{2}{3r_s C} \int_0^\tau \zeta^2(x) dx} d\tau \right]. \quad (2.7)$$

If the active filter is connected to a network with infinite power, the space vector of the voltage \mathbf{v}_s is equal to:

$$\mathbf{v}_s = V_s e^{j\omega t + j\varphi}$$

and then eq. (2.6) gives the final form of the solution:

$$\mathbf{i}_s(t) = -\frac{V_s}{r_s} e^{j\omega t} + \frac{2}{3r_s} \zeta(t) e^{j\frac{\pi}{3}\eta(t) - \frac{2}{3r_s C} \int_0^t \zeta^2(x) dx} \left\{ \mathbf{v}_{dc0} + \frac{V_s}{r_s C} \int_0^t \zeta(\tau) \cos \left[\omega \tau + \varphi - \frac{\pi}{3} \eta(\tau) \right] e^{\frac{2}{3r_s C} \int_0^\tau \zeta^2(x) dx} d\tau \right\}. \quad (2.8)$$

II.3.a. Square-wave inverters

Square wave inverter operations imply that $\zeta(t) = I$ and $\eta(t) = [6t / T]$ and therefore the integrals appearing in eq. (2.6), and subsequently in eq. (2.7), can be analytically solved. If the following change of variable is performed:

$$t = \frac{T}{6}(n+m)$$

and it is $\tau = 3r_s C / 2$, the eq. (2.6) yields:

$$\mathbf{v}_{dc}(n,m) = e^{-\frac{T}{6\tau}(n+m)} \left\{ \frac{V_s \pi}{2\tau \omega} \left[\sum_{k=0}^{n-1} \left(\int_0^1 \cos \left(\frac{\pi}{3} m + \varphi \right) e^{\frac{\pi}{3\omega\tau} m} dm \right) e^{\frac{\pi}{3\omega\tau} k} + \frac{\pi}{3\omega} \int_0^m \cos \left(\frac{\pi}{3} x + \varphi \right) e^{\frac{\pi}{3\omega\tau} x} dx \right] + \mathbf{v}_{dc0} \right\}.$$

The calculation of the integrals in the variable m and the summation in the variable n indicated in the previous equation leads to the final expression of the dc-link voltage:

$$v_{dc}(n,m) = e^{-\frac{\pi}{3\omega\tau}(n+m)} v_{dc0} + \frac{3V_s}{2} \frac{I}{I + (\omega\tau)^2} \left\{ e^{-\frac{\pi}{3\omega\tau}m} \frac{e^{-\frac{\pi}{3\omega\tau}n} - I}{e^{-\frac{\pi}{3\omega\tau}n} - I} \times \right. \\ \times \left[\cos\left(\frac{\pi}{3}m + \varphi\right) + \omega\tau \sin\left(\frac{\pi}{3}m + \varphi\right) + e^{-\frac{\pi}{3\omega\tau}} (\cos\varphi + \omega\tau \sin\varphi) \right] + \quad (2.9) \\ \left. + \cos\left(\frac{\pi}{3}m + \varphi\right) + \omega\tau \sin\left(\frac{\pi}{3}m + \varphi\right) - e^{-\frac{\pi}{3\omega\tau}m} (\cos\varphi + \omega\tau \sin\varphi) \right\}.$$

Putting also $\tan(\psi) = \omega\tau$ and rearranging the terms, the eq. (2.9) yields:

$$v_{dc}(n,m) = e^{-\frac{\pi}{3\omega\tau}(n+m)} v_{dc0} + \frac{3V_s}{2} \cos\psi \left\{ \cos\left(\frac{\pi}{3}m + \varphi - \psi\right) + \right. \\ \left. + e^{-\frac{\pi}{3\omega\tau}(n+m)} \frac{e^{-\frac{\pi}{3\omega\tau}} \cos(\varphi - \psi) + \sin(\varphi - \psi)}{1 - e^{-\frac{\pi}{3\omega\tau}}} + \right. \\ \left. + \frac{\cos\left(\frac{\pi}{3} + \varphi - \psi\right) - \cos(\varphi - \psi)}{1 - e^{-\frac{\pi}{3\omega\tau}}} e^{-\frac{\pi}{3\omega\tau}m} \right\}. \quad (2.10)$$

The eq. (2.10) clearly shows that the dynamic response of the dc-link voltage does not depend separately on the values of the filter resistance, r_s , nor on the dc-link capacitance, C , but only on the time constant $\tau = 3 r_s C / 2$.

The final expression of the current i_s can be also easily evaluated from eq. (2.8):

$$i_s(n,m) = -\frac{V_s}{r_s} e^{j\frac{\pi}{3}(n+m)+j\varphi} + \frac{2}{3r_s} e^{j\frac{\pi}{3}n - \frac{\pi}{3\omega\tau}(n+m)} v_{dc0} + \frac{V_s}{r_s} e^{j\frac{\pi}{3}n} \cos\psi \times \\ \times \left\{ \cos\left(\frac{\pi}{3}m + \varphi - \psi\right) + \frac{e^{-\frac{\pi}{3\omega\tau}} \cos(\varphi - \psi) + \sin(\varphi - \psi)}{\left(1 - e^{-\frac{\pi}{3\omega\tau}}\right)} e^{-\frac{\pi}{3\omega\tau}(n+m)} + \quad (2.11) \right. \\ \left. + \frac{\cos\left(\frac{\pi}{3} + \varphi - \psi\right) - \cos(\varphi - \psi)}{\left(1 - e^{-\frac{\pi}{3\omega\tau}}\right)} e^{-\frac{\pi}{3\omega\tau}m} \right\}.$$

The steady-state expressions of the dc-link voltage and the ac current can be evaluated respectively from eqs. (2.10)

and (2.11) making the limit for $n \rightarrow \infty$.

$$\tilde{v}_{dc}(m) = \frac{3V_s}{2} \cos \psi \left[\cos\left(\frac{\pi}{3}m + \varphi - \psi\right) + \frac{\cos\left(\frac{\pi}{3} + \varphi - \psi\right) - \cos(\varphi - \psi)}{\left(1 - e^{-\frac{\pi}{3\omega\tau}}\right)} e^{-\frac{\pi}{3\omega\tau}m} \right], \quad (2.12)$$

$$\tilde{i}_s(\tilde{n}, m) = -\frac{V_s}{r_s} e^{j\frac{\pi}{3}(\tilde{n}+m)+j\varphi} + \frac{V_s}{r_s} e^{j\frac{\pi}{3}\tilde{n}} \cos \psi \times \left[\cos\left(\frac{\pi}{3}m + \varphi - \psi\right) + \frac{\cos\left(\frac{\pi}{3} + \varphi - \psi\right) - \cos(\varphi - \psi)}{\left(1 - e^{-\frac{\pi}{3\omega\tau}}\right)} e^{-\frac{\pi}{3\omega\tau}m} \right], \quad (2.13)$$

where \tilde{n} is the periodic replica of the restriction of the function n to the first six steps. Eqs. (2.12) and (2.13) show indeed that at steady-state the dc-link is periodic of $T/6$, whereas the current is periodic of T .

The mean value of the dc-link voltage can be evaluated by eq. (2.12) as follow:

$$\begin{aligned} \tilde{V}_{dc} &= \frac{1}{T} \int_0^T \tilde{v}_{dc}(t) dt = \frac{1}{6} \sum_{k=0}^{n-1} \int_0^l \tilde{v}_{dc}(m) dm = \int_0^l \tilde{v}_{dc}(m) dm = \\ &= \frac{3V_s}{2} \frac{3}{\pi} \cos \psi \left[\sin\left(\frac{\pi}{3} + \varphi - \psi\right) - \sin(\varphi - \psi) + \right. \\ &\quad \left. + \omega\tau \cos\left(\frac{\pi}{3} + \varphi - \psi\right) - \omega\tau \cos(\varphi - \psi) \right] = \\ &= \frac{9}{2\pi} V_s \sin\left(\frac{\pi}{3} - \varphi\right). \end{aligned} \quad (2.14)$$

The eq. (2.14) points out that the mean value of dc-voltage is independent on the values of passive filter elements, whereas it depends on the phase shift between the square-wave and the mains voltage with sinusoidal law.

Another quantity of interest is the ripple of the dc-link voltage, which is given by:

$$\Delta V_{dc} = \tilde{v}_{dc,max} - \tilde{v}_{dc,min} = \tilde{v}_{dc}(\bar{m}) - \tilde{v}_{dc}(0)$$

The value \bar{m} can be immediately evaluated from (2.12) putting the derivative respect to m equal to 0:

$$-\frac{\pi}{3} \sin\left(\frac{\pi}{3}\bar{m} + \varphi - \psi\right) = \frac{\pi}{3\omega\tau} \frac{\cos\left(\frac{\pi}{3} + \varphi - \psi\right) - \cos(\varphi - \psi)}{\left(1 - e^{-\frac{\pi}{3\omega\tau}}\right)} e^{-\frac{\pi}{3\omega\tau}\bar{m}}, \quad (2.15)$$

where $0 \leq \bar{m} \leq l$. The eq. (2.15) can be easily solved using a numerical routine and then the ripple can be easily found substituting the value \bar{m} in eq. (2.12).

II.3.b. Numerical results with inverter driven by square-wave control

In order to show the dynamical evolution of the quantities of interests, the transients due to the sudden

connection of an active filter in parallel to the network have been considered. The transients have been evaluated with zero initial condition of v_{dc} and different time constants τ , with the same r_s , and the diagrams of fig.2.2 have been obtained.

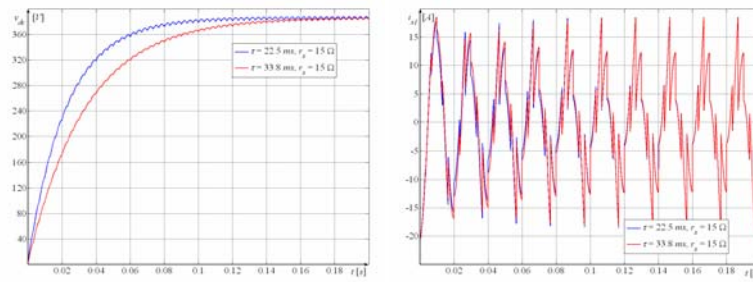


Fig.2.2. Transients of dc-link voltage and ac current after a sudden connection to the mains

Fig.2.2 confirms that the steady-state conditions are reached after 4 - 5 times the time constants τ , which are in the case considered

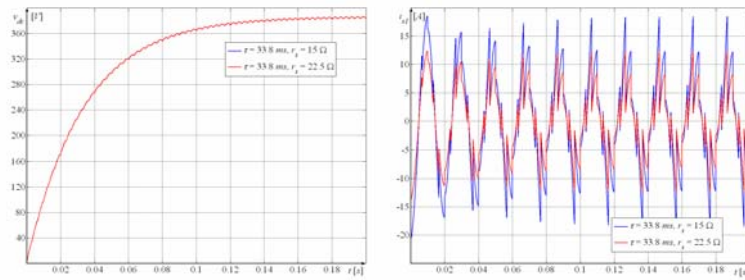


Fig.2.3. Transients of dc-link voltage and ac current with the same τ and C but different r_s .

respectively equal to 22.5 ms (blue trace) and 33.8 ms (red trace). As predicted by eq. (2.14), the mean value of the dc-link voltage is independent on τ . Reminding the eq. (2.13), it is also clear that the steady-state waveforms of the currents are the same, because the filter resistances are equal.

In the following figs.2.3, the transients of the sudden connection of the filter to the network are shown. The analytical evaluation of the quantities of interest has been carried out with the same τ , different resistances and zero initial conditions. It can be noticed that the dc voltage is the same, whereas the current diagram is scaled of the resistance ratio.

In the figs.2.4 other transients with the same time constant but different phase displacement are compared. Figs.2.4 put in evidence that in the two examples considered the dynamic responses of v_{dc} and i_s are the same because the time constants are equal. However, the different phase displacement influences not only the amplitude and the phase shift of the current, but also the mean value and the ripple of v_{dc} . In particular, the dependence of these two quantities on the variable φ has shown in the next figs.2.5.

It has been also investigated the dependence on the phase

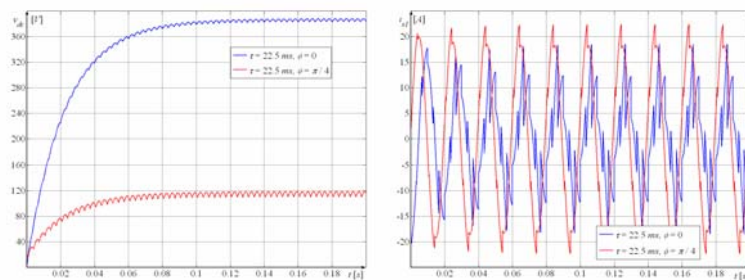


Fig.2.4. Transients of dc-link voltage and ac current with the same r_s and C but different φ

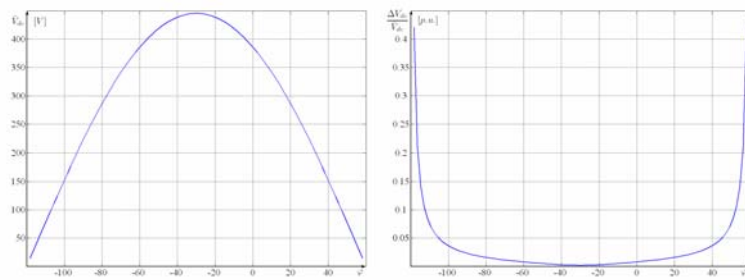


Fig.2.5. Mean value and ripple referred to its mean value of the dc-link voltage

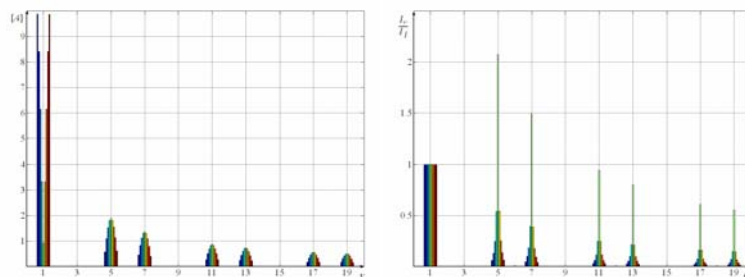


Fig.2.6. Current harmonics in absolute value and relative value changing φ

displacement φ of the harmonics of the current. This is shown in figs.2.6, where are represented the harmonic currents both in absolute value and in per unit respect to the fundamental. As figs.2.6 clearly put in evidence, the harmonic content of the current is strongly dependent on φ . If φ is -30° , the first harmonic is very small, whereas other harmonics reach their maximum. For values of φ different from -30° , the situation is symmetric respect to -30° . It can be noticed that the fundamental increases in a large range when φ increases and, instead, the other harmonics decrease. For values of φ equal to -120° and 60° the harmonics are all nil, the current becomes sinusoidal and reaches its maximum amplitude V_s / r_s . This can be easily explained because for these φ the mean value of the voltage across the dc-link capacitor is zero and then the filter resistors are short-circuited. The harmonic analysis shows that the square-wave control allows the filter the reactive power compensation, achieved selecting the suitable value of φ . The harmonic content can be also regulated with the control of φ , even though the harmonics are always in the same ratio among each other. This involves that the square-wave is a suitable control technique only if such a compensation for harmonics is required.

Another important aspect that an analytical solution can easily highlight is how voltages and currents are dependent on the passive filter parameters. The ripple of v_{dc} as a function of the phase displacement φ

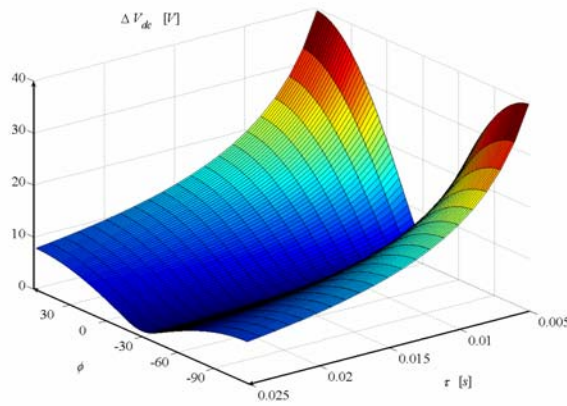


Fig.2.7. Ripple of the dc-link voltage as a function of parameters φ and τ

and the time constant τ is shown in the following fig.2.7. As it can be seen, the ripple is very low in the whole range of φ for τ greater than 15 ms. The same analysis has been performed for the rms value of the filter current respect to the parameters r_s and C . The figs.2.8 shows that $I_{s,rms}$ is in practice independent on C . Conversely, the rms current can be changed in a wide range properly selecting the value of r_s . Moreover, the analysis points out that the variation of the parameter φ can be successfully used for the control of the ac filter current.

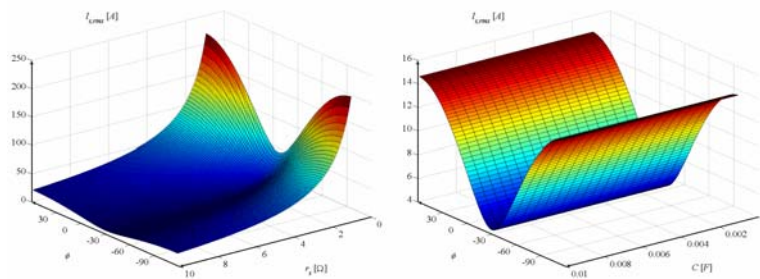


Fig.2.8. Rms currents as a function of φ and r_s (a), and φ and C (b)

II.4. ACTIVE FILTER WITH INDUCTANCES DRIVEN WITH SQUARE-WAVE CONTROL

Square wave inverter operations imply that $\xi(t) = I$ and $\eta(t) = [6t / T]$ and therefore their time derivative in the system of eqs. (2.4) can be evaluated:

$$\frac{d\xi}{dt} = 0 ;$$

$$\frac{d}{dt} e^{-j\frac{\pi}{3}\eta(t)} = \sum_{n=0}^{+\infty} e^{-j\frac{\pi}{3}(n+2)} \delta \left[t - (n+1)\frac{T}{6} \right].$$

As it can be seen, square-wave operations imply the derivative of a discontinuous time function. The sampling property of the Dirac Delta function leads to the following expression:

$$\mathbf{y} e^{j\frac{\pi}{3}\eta(t)} \frac{d}{dt} e^{-j\frac{\pi}{3}\eta(t)} = \sum_{n=0}^{+\infty} e^{-j\frac{\pi}{3}} \mathbf{y} \left[(n+1)\frac{T}{6} \right] \delta \left[t - (n+1)\frac{T}{6} \right].$$

The system of eq.s (2.4), hence, becomes:

$$\left\{ \begin{array}{l} \mathbf{v}'_s + r_s \mathbf{y} + l_s \frac{d\mathbf{y}}{dt} - l_s \sum_{n=0}^{+\infty} e^{-j\frac{\pi}{3}} \mathbf{y} \left[(n+1)\frac{T}{6} \right] \times \\ \times \delta \left[t - (n+1)\frac{T}{6} \right] = \frac{2}{3} \mathbf{v}_{dc}; \\ \frac{d\mathbf{v}_{dc}}{dt} = -\frac{1}{C} \text{Re}\{\mathbf{y}\}. \end{array} \right. \quad (2.16)$$

It is difficult to achieve a closed solution of system of eqs. (2.16) by using ordinary solving techniques. However, the form of the equations suggests to find a solution by means of an integral transformation. The modified z -transform seems to be the most suitable solving technique to this kind of problem.

II.4.a. The modified z -transform method

In many discrete systems, flowing signals are considered at discrete values of the time, usually for $t = nT$, with $n = 0, 1, 2, \dots$, and with T fixed positive number, usually defined “sampling period”. The analysis of such discrete systems may be carried through by using the z -transform method. In some applications, the output between the sampling instants is very important and, thus, the z -transform method is not quite adequate for a critical study of such systems. However, the z -transform can be easily modified to cover the system behaviour at all instants of time; such an extension of the method is called “modified z -transform”. To obtain the values of $f(t)$ other than at the sampling instants $t = nT$, the following change of variables can be performed:

$$t = (n-1+m)T, \quad n = 0, 1, 2, K, \quad 0 \leq m < 1$$

The definition of the modified z -transform of the time function f is [11]:

$$\mathbf{F}(z, m) = z^{-l} \sum_{n=0}^{\infty} f[(n+m)T] z^{-n}. \quad (2.17)$$

The relationship between the modified z -transform and the z -transform can be easily obtained by putting $m = 0$. It is, in fact:

$$z\mathbf{F}(z, 0) = \sum_{n=0}^{\infty} f(nT) z^{-n} = F(z) \quad (2.18)$$

In some applications it is useful to evaluate the modified z -transform of a function $f(t)$ starting from its Laplace transform rather than directly from eqs. (2.17). The relationship between the modified z -transform and the Laplace

transform $F(s)$ is:

$$F(z, m) \Big|_{z=e^{Ts}} = \frac{1}{2j\pi} z^{-1} \int_{c-j\infty}^{c+j\infty} F(p) e^{mpT} \frac{1}{1-e^{-T(s-p)}} dp, \quad 0 \leq m < 1. \quad (2.19)$$

Integrating in the left-half plane and assuming $F(s)$ has regular singularities, eq. (2.19) becomes:

$$F(z, m) = z^{-1} \sum_{\substack{\text{poles of} \\ F(s)}} \text{residue of } \frac{F(s) e^{msT}}{1-e^{sT} z^{-1}}, \quad 0 \leq m < 1 \quad (2.20)$$

where the summation is extended only to the poles of $F(s)$ because the other poles are in the right-half plane. When $F(s) = A(s) / B(s)$ has simple poles, eq. (2.20) can be expressed as:

$$F(z, m) = z^{-1} \sum_{n=1}^N \frac{A(s_n)}{B'(s_n)} \frac{e^{ms_n T}}{1-e^{s_n T} z^{-1}}, \quad 0 \leq m < 1 \quad (2.21)$$

where s_1, s_2, \dots, s_n are the simple roots of $B(s) = 0$.

II.4.b. The application of the modified z-transform to active filters

In order to use the method of the modified z-transform, system of eqs. (2.8) has been transformed by Laplace. These Laplace transforms are complex functions of the variable $s = x + iz$, defined in a complex plane, which is, obviously, different from $\{\Re, j \Im\}$. For sake of simplicity, if all initial conditions are considered to be nil, there results:

$$\left\{ \begin{array}{l} V'_s(s) + r_s Y(s) + l_s s Y(s) - l_s \sum_{n=0}^{+\infty} e^{-j\frac{\pi}{3}} y \left[(n+1) \frac{T}{6} \right] \times \\ \times e^{-(n+1)\frac{T}{6}s} = \frac{2}{3} V_{dc}(s) \\ s V_{dc}(s) = -\frac{1}{C} \text{Re}\{Y(s)\} \end{array} \right. \quad (2.22)$$

Real and imaginary parts of eqs. (2.22) make it possible to solve for $Y_r(s)$ and $Y_i(s)$:

$$Y_r(s) = \frac{s}{s^2 + \frac{r_s}{l_s} s + \frac{2}{3l_s C}} \left(-\frac{V'_{sr}(s)}{l_s} + \sum_{n=0}^{+\infty} e^{-(n+1)\frac{T}{6}s} \left\{ \frac{1}{2} y_r \left[(n+1) \frac{T}{6} \right] + \frac{\sqrt{3}}{2} y_i \left[(n+1) \frac{T}{6} \right] \right\} \right), \quad (2.23)$$

$$Y_i(s) = \frac{1}{s + \frac{r_s}{l_s}} \left(-\frac{V'_{si}(s)}{l_s} + \sum_{n=0}^{+\infty} e^{-(n+1)\frac{T}{6}s} \left\{ -\frac{\sqrt{3}}{2} y_r \left[(n+1) \frac{T}{6} \right] + \frac{1}{2} y_i \left[(n+1) \frac{T}{6} \right] \right\} \right).$$

By putting:

$$k_{1,2} = \frac{T}{6} \left(-\frac{r_s}{2l_s} \pm \sqrt{\left(\frac{r_s}{2l_s}\right)^2 - \frac{2}{3l_s C}} \right) = \frac{T}{6} \frac{r_s}{2l_s} \left(-1 \pm \sqrt{1 - 4 \frac{l_s}{r_s} \frac{2}{3r_s C}} \right)$$

eqs. (2.23) assume the following expressions:

$$Y_r(s) = \frac{s}{\left(s - \frac{6}{T}k_1\right)\left(s - \frac{6}{T}k_2\right)} \left\langle -\frac{V'_{sr}(s)}{l_s} + \sum_{n=0}^{+\infty} e^{-\frac{(n+1)T}{6}s} \left\{ \frac{1}{2}y_r \left[(n+1)\frac{T}{6} \right] + \frac{\sqrt{3}}{2}y_i \left[(n+1)\frac{T}{6} \right] \right\} \right\rangle \quad (2.24)$$

$$Y_i(s) = \frac{l}{\left[s - \frac{6}{T}(k_1 + k_2)\right]} \left\langle -\frac{V'_{si}(s)}{l_s} + \sum_{n=0}^{+\infty} e^{-\frac{(n+1)T}{6}s} \left\{ -\frac{\sqrt{3}}{2}y_r \left[(n+1)\frac{T}{6} \right] + \frac{1}{2}y_i \left[(n+1)\frac{T}{6} \right] \right\} \right\rangle$$

Eqs. (2.24) show that inner filter parameters influence $Y_r(s)$ and $Y_i(s)$ and, hence, the physical response of the filter only in terms of quantities $\alpha = l_s / r_s$ and $\beta = 3 r_s C / 2$.

In order to obtain the modified z -transforms of eqs. (2.24) it should be noted that eq. (2.21) can be used putting $s = 6/T \ln z$. Moreover, it has to be considered that:

$$\begin{aligned} Z_m \left\{ \sum_{n=0}^{+\infty} e^{-\frac{(n+1)T}{6}s} y_r \left[(n+1)\frac{T}{6} \right] \right\} &= \sum_{n=0}^{+\infty} y_r \left[(n+1)\frac{T}{6} \right] z^{-(n+1)} = \\ &= \sum_{k=0}^{+\infty} y_r \left(k \frac{T}{6} \right) z^{-k} - y_r(0) = Y_r(z) . \end{aligned}$$

An analogue transformation is valid for y_i . Finally, writing in block letters the z -transforms and in script letters the modified z -transforms, there results:

$$\begin{aligned} \mathbf{Y}_r(z, m) &= \mathbf{F}(z, m) + \\ &+ \left[\frac{1}{2}Y_r(z) + \frac{\sqrt{3}}{2}Y_i(z) \right] \frac{l}{k_1 - k_2} \left(\frac{k_1 e^{k_1 m}}{z - e^{k_1}} - \frac{k_2 e^{k_2 m}}{z - e^{k_2}} \right) ; \\ \mathbf{Y}_i(z, m) &= \mathbf{G}(z, m) + \\ &+ \left[-\frac{\sqrt{3}}{2}Y_r(z) + \frac{1}{2}Y_i(z) \right] \frac{e^{(k_1+k_2)m}}{z - e^{(k_1+k_2)}} , \end{aligned} \quad (2.25)$$

where, for simplicity of notation, it has been put:

$$\mathbf{F}(z, m) = \mathbf{Z}_m \left\{ -\frac{s}{\left(s - \frac{6}{T}k_1\right)\left(s - \frac{6}{T}k_2\right)} \frac{V'_{sr}(s)}{l_s} \right\}, \quad (2.26)$$

$$\mathbf{G}(z, m) = \mathbf{Z}_m \left\{ -\frac{I}{\left[s - \frac{6}{T}(k_1 + k_2)\right]} \frac{V'_{si}(s)}{l_s} \right\}.$$

When, moreover, supplied voltages are sinusoidal, there results:

$$\begin{aligned} V'_s(s) &= \mathbf{L} \left\{ \mathbf{v}_s e^{-j\frac{\pi}{3}\left[\frac{6t}{T}\right]} \right\} = \mathbf{L} \left\{ V_s e^{j(\omega t + \varphi)} e^{-j\frac{\pi}{3}\left[\frac{6t}{T}\right]} \right\} = \\ &= V_s e^{j\varphi} \frac{e^{\frac{T}{6}s} - e^{j\frac{\pi}{3}}}{\left(e^{\frac{T}{6}s} - 1\right)\left(s - j\frac{\pi}{3}\frac{6}{T}\right)}. \end{aligned} \quad (2.27)$$

If the source voltage is polluted by harmonics, the analysis is still possible with the same method. The only condition required is that the source voltage is a periodic function, whose period is the same of the square-wave control.

Taking into account eqs. (2.21) and (2.27), eqs. (2.26) can be written as follows:

$$\begin{aligned} \mathbf{F}(z, m) &= -\frac{\frac{V_s T}{l_s 6}}{z-1} \left[\frac{\left(\frac{\pi^2}{9} - k_1 k_2\right) \sin\left(\frac{\pi}{3}m + \varphi\right) - \frac{\pi}{3}(k_1 + k_2) \cos\left(\frac{\pi}{3}m + \varphi\right)}{\frac{3}{\pi}\left(k_1^2 + \frac{\pi^2}{9}\right)\left(k_2^2 + \frac{\pi^2}{9}\right)} + \right. \\ &+ \frac{k_1}{k_1 - k_2} \frac{e^{k_1 m}}{z - e^{k_1}} \frac{\left(k_1 \cos \varphi - \frac{\pi}{3} \sin \varphi\right) z + \frac{\pi}{3} \sin\left(\varphi + \frac{\pi}{3}\right) - k_1 \cos\left(\varphi + \frac{\pi}{3}\right)}{\left(k_1^2 + \frac{\pi^2}{9}\right)} + \quad \text{and} \\ &\left. - \frac{k_2}{k_1 - k_2} \frac{e^{k_2 m}}{z - e^{k_2}} \frac{\left(k_2 \cos \varphi - \frac{\pi}{3} \sin \varphi\right) z + \frac{\pi}{3} \sin\left(\varphi + \frac{\pi}{3}\right) - k_2 \cos\left(\varphi + \frac{\pi}{3}\right)}{\left(k_2^2 + \frac{\pi^2}{9}\right)} \right] \\ \mathbf{G}(z, m) &= \frac{\frac{V_s T}{l_s 6}}{z-1} \left\{ \frac{\left(k_1 + k_2\right) \sin\left(\frac{\pi}{3}m + \varphi\right) + \frac{\pi}{3} \cos\left(\frac{\pi}{3}m + \varphi\right)}{\left(k_1 + k_2\right)^2 + \frac{\pi^2}{9}} + \frac{e^{(k_1 + k_2)m}}{z - e^{k_1 + k_2}} \times \right. \\ &\times \left. \frac{\left[\left(k_1 + k_2\right) \sin \varphi + \frac{\pi}{3} \cos \varphi\right] z - \left(k_1 + k_2\right) \sin\left(\varphi + \frac{\pi}{3}\right) - \frac{\pi}{3} \cos\left(\varphi + \frac{\pi}{3}\right)}{\left(k_1 + k_2\right)^2 + \frac{\pi^2}{9}} \right\}. \end{aligned}$$

Rearranging the previous equations and putting:

$$\sin\gamma = \frac{\left(\frac{\pi^2}{9} - k_1 k_2\right)}{\sqrt{\left(k_1^2 + \frac{\pi^2}{9}\right)\left(k_2^2 + \frac{\pi^2}{9}\right)}}; \quad \cos\gamma = \frac{\frac{\pi}{3}(k_1 + k_2)}{\sqrt{\left(k_1^2 + \frac{\pi^2}{9}\right)\left(k_2^2 + \frac{\pi^2}{9}\right)}};$$

$$\sin\delta = \frac{\frac{\pi}{3}}{\sqrt{\left(k_1^2 + \frac{\pi^2}{9}\right)}}; \quad \cos\delta = \frac{k_1}{\sqrt{\left(k_1^2 + \frac{\pi^2}{9}\right)}};$$

$$\sin\varepsilon = \frac{\frac{\pi}{3}}{\sqrt{\left(k_2^2 + \frac{\pi^2}{9}\right)}}; \quad \cos\varepsilon = \frac{k_2}{\sqrt{\left(k_2^2 + \frac{\pi^2}{9}\right)}};$$

$$\sin\zeta = \frac{\frac{\pi}{3}}{\sqrt{(k_1 + k_2)^2 + \frac{\pi^2}{9}}}; \quad \cos\zeta = \frac{k_1 + k_2}{\sqrt{(k_1 + k_2)^2 + \frac{\pi^2}{9}}}$$

there results:

$$\mathbf{F}(z, m) = -\frac{l}{z-1} \frac{V_s}{r_s} \left[\cos\gamma \cos\left(\frac{\pi}{3}m + \varphi + \gamma\right) + \cos\delta \frac{e^{k_1 m}}{z - e^{k_1}} \frac{\cos(\varphi + \delta)z - \cos\left(\varphi + \delta + \frac{\pi}{3}\right)}{\sqrt{1 - 4\frac{\alpha}{\beta}}} + \cos\varepsilon \frac{e^{k_2 m}}{z - e^{k_2}} \frac{\cos(\varphi + \varepsilon)z - \cos\left(\varphi + \varepsilon + \frac{\pi}{3}\right)}{\sqrt{1 - 4\frac{\alpha}{\beta}}} \right]$$

and

$$\mathbf{G}(z, m) = \frac{l}{z-1} \frac{V_s}{r_s} \cos\zeta \left\{ -\sin\left(\frac{\pi}{3}m + \varphi + \zeta\right) + \frac{e^{(k_1+k_2)m}}{z - e^{k_1+k_2}} \left[\sin(\varphi + \zeta)z - \sin\left(\varphi + \frac{\pi}{3} + \zeta\right) \right] \right\}.$$

It should be noted that in the system of eqs. (2.25) both the z -transforms and the modified z -transforms of the unknown quantities appear. To solve the problem completely, eqs. (2.18) of the modified z -transform may be used:

$$\begin{cases} Y_r(z) = z \mathbf{Y}_r(z, 0) \\ Y_i(z) = z \mathbf{Y}_i(z, 0) \end{cases} \quad (2.28)$$

Therefore, by means of eqs. (2.28) the following algebraic system is obtained:

$$Y_r(z) = z\mathbf{F}(z,0) + \left[\frac{1}{2}Y_r(z) + \frac{\sqrt{3}}{2}Y_i(z) \right] \frac{z}{k_1 - k_2} \left(\frac{k_1}{z - e^{k_1}} - \frac{k_2}{z - e^{k_2}} \right); \quad (2.29)$$

$$Y_i(z) = z\mathbf{G}(z,0) + \left[-\frac{\sqrt{3}}{2}Y_r(z) + \frac{1}{2}Y_i(z) \right] \frac{z}{z - e^{k_1+k_2}}.$$

The resolution of algebraic system (2.29) allows for the evaluation of $Y_r(z)$ and $Y_i(z)$:

$$Y_r(z) = \frac{z \left[(k_1 - k_2)(z - 2e^{k_1+k_2})\mathbf{F}(z,0) + \sqrt{3}z(z - e^{k_1+k_2}) \left(\frac{k_1}{z - e^{k_1}} - \frac{k_2}{z - e^{k_2}} \right) \mathbf{G}(z,0) \right]}{\frac{k_1}{z - e^{k_1}} \left[z(2z - e^{k_1}) - e^{k_1+k_2}(z - 2e^{k_1}) \right] + \frac{k_2}{z - e^{k_2}} \left[z(2z - e^{k_2}) - e^{k_1+k_2}(z - 2e^{k_2}) \right]} \quad (2.30)$$

$$Y_i(z) = \frac{z \left[(z - e^{k_1+k_2}) \left(k_1 \frac{z - 2e^{k_1}}{z - e^{k_1}} - k_2 \frac{z - 2e^{k_2}}{z - e^{k_2}} \right) \mathbf{G}(z,0) - \sqrt{3}z(k_1 - k_2)\mathbf{F}(z,0) \right]}{\frac{k_1}{z - e^{k_1}} \left[z(2z - e^{k_1}) - e^{k_1+k_2}(z - 2e^{k_1}) \right] + \frac{k_2}{z - e^{k_2}} \left[z(2z - e^{k_2}) - e^{k_1+k_2}(z - 2e^{k_2}) \right]}$$

By performing the inverse z -transform, the sequences of values at each sampling time $y_r\left(n\frac{T}{6}\right)$ and $y_i\left(n\frac{T}{6}\right)$ can be, hence, obtained. By substituting eqs. (2.30) in the system (2.25), the solution in terms of modified z -transforms can be finally achieved:

$$\mathbf{Y}_r(z,m) = \frac{z \left[\mathbf{F}(z,0)(z + e^{k_1+k_2}) + \sqrt{3}\mathbf{G}(z,0)(z - e^{k_1+k_2}) \right] \times \left(\frac{k_1 e^{k_1 m}}{z - e^{k_1}} - \frac{k_2 e^{k_2 m}}{z - e^{k_2}} \right)}{\frac{k_1}{z - e^{k_1}} \left[z(2z - e^{k_1}) - e^{k_1+k_2}(z - 2e^{k_1}) \right] + \frac{k_2}{z - e^{k_2}} \left[z(2z - e^{k_2}) - e^{k_1+k_2}(z - 2e^{k_2}) \right]} + \mathbf{F}(z,m) \quad (2.31)$$

$$\mathbf{Y}_i(z,m) = \frac{z \left[-\sqrt{3}\mathbf{F}(z,0)(k_1 - k_2) - \mathbf{G}(z,0) \left(k_1 \frac{z + e^{k_1}}{z - e^{k_1}} - k_2 \frac{z + e^{k_2}}{z - e^{k_2}} \right) \right] e^{(k_1+k_2)m}}{\frac{k_1}{z - e^{k_1}} \left[z(2z - e^{k_1}) - e^{k_1+k_2}(z - 2e^{k_1}) \right] + \frac{k_2}{z - e^{k_2}} \left[z(2z - e^{k_2}) - e^{k_1+k_2}(z - 2e^{k_2}) \right]} + \mathbf{G}(z,m)$$

The continuous time functions $y_r(n,m)$ and $y_i(n,m)$ may be obtained from the modified z -transforms $\mathbf{Y}_r(z,m)$ and

$\mathbf{Y}_i(z,m)$ by the inverse modified z -transformation process. Eq. (2.3) gives in the end the complex time function $\mathbf{i}_s(n,m)$:

$$\mathbf{i}_s(n,m) = [y_r(n,m) + j y_i(n,m)] e^{j \frac{\pi}{3} n}$$

In some applications, it is useful to know the behaviour of the active filter only in steady-state conditions. The steady-state solution can be easily carried out with the modified z -transform. Indeed, only the steady-state limits of the above mentioned sequences are necessary. According to the z -transform final value theorem [11], they are given by the following limits:

$$\tilde{y}_r(m) = \lim_{z \rightarrow 1} (z-1) \mathbf{Y}_r(z,m)$$

$$\tilde{y}_i(m) = \lim_{z \rightarrow 1} (z-1) \mathbf{Y}_i(z,m)$$

and therefore:

$$\begin{aligned} \tilde{y}_r(m) = \tilde{F}(m) + & \frac{\left[-\tilde{F}(0)(1 + e^{k_1+k_2}) + \sqrt{3}\tilde{G}(0)(1 - e^{k_1+k_2}) \right] \times \\ & \times \left(\frac{k_1 e^{k_1 m} - k_2 e^{k_2 m}}{1 - e^{k_1} - 1 - e^{k_2}} \right)}{\frac{k_1}{1 - e^{k_1}} \left[(2 - e^{k_1}) - e^{k_1+k_2} (1 - 2e^{k_1}) \right] + \\ & - \frac{k_2}{1 - e^{k_2}} \left[(2 - e^{k_2}) - e^{k_1+k_2} (1 - 2e^{k_2}) \right]} \end{aligned} \quad (2.32)$$

$$\begin{aligned} \tilde{y}_i(m) = \tilde{G}(m) + & \frac{\left[-\sqrt{3}\tilde{F}(0)(k_1 - k_2) + \right. \\ & \left. - \tilde{G}(0) \left(k_1 \frac{1 + e^{k_1}}{1 - e^{k_1}} - k_2 \frac{1 + e^{k_2}}{1 - e^{k_2}} \right) \right] e^{(k_1+k_2)m}}{\frac{k_1}{1 - e^{k_1}} \left[(2 - e^{k_1}) - e^{k_1+k_2} (1 - 2e^{k_1}) \right] + \\ & - \frac{k_2}{1 - e^{k_2}} \left[(2 - e^{k_2}) - e^{k_1+k_2} (1 - 2e^{k_2}) \right]} \end{aligned}$$

where it has been denoted by:

$$\begin{aligned} \tilde{F}(m) = -\frac{V_s}{r_s} & \left[\cos\gamma \cos\left(\frac{\pi}{3}m + \varphi + \gamma\right) + \cos\delta \frac{e^{k_1 m}}{1 - e^{k_1}} \frac{\sin\left(\varphi + \delta + \frac{\pi}{6}\right)}{\sqrt{1 - 4\frac{\alpha}{\beta}}} + \right. \\ & \left. - \cos\varepsilon \frac{e^{k_2 m}}{1 - e^{k_2}} \frac{\sin\left(\varphi + \varepsilon + \frac{\pi}{6}\right)}{\sqrt{1 - 4\frac{\alpha}{\beta}}} \right] \end{aligned}$$

$$\tilde{G}(m) = -\frac{V_s}{r_s} \cos\zeta \left[\sin\left(\frac{\pi}{3}m + \varphi + \zeta\right) + \frac{e^{(k_1+k_2)m}}{1 - e^{k_1+k_2}} \cos\left(\varphi + \zeta + \frac{\pi}{6}\right) \right]$$

The steady-state values of the sequences $y_r\left(n\frac{T}{6}\right)$ and $y_i\left(n\frac{T}{6}\right)$ can be easily evaluated putting in eqs. (2.32) $m = 0$:

$$\begin{aligned}
 y_{rss} &= \tilde{F}(0) + \frac{\left[-\tilde{F}(0)(1 + e^{k_1+k_2}) + \sqrt{3}\tilde{G}(0)(1 - e^{k_1+k_2}) \right] \times \left(\frac{k_1}{1 - e^{k_1}} - \frac{k_2}{1 - e^{k_2}} \right)}{\frac{k_1}{1 - e^{k_1}} \left[(2 - e^{k_1}) - e^{k_1+k_2}(1 - 2e^{k_1}) \right] + \frac{k_2}{1 - e^{k_2}} \left[(2 - e^{k_2}) - e^{k_1+k_2}(1 - 2e^{k_2}) \right]} \\
 y_{iss} &= \tilde{G}(0) + \frac{\left[-\sqrt{3}\tilde{F}(0)(k_1 - k_2) - \tilde{G}(0) \left(k_1 \frac{1 + e^{k_1}}{1 - e^{k_1}} - k_2 \frac{1 + e^{k_2}}{1 - e^{k_2}} \right) \right]}{\frac{k_1}{1 - e^{k_1}} \left[(2 - e^{k_1}) - e^{k_1+k_2}(1 - 2e^{k_1}) \right] + \frac{k_2}{1 - e^{k_2}} \left[(2 - e^{k_2}) - e^{k_1+k_2}(1 - 2e^{k_2}) \right]}
 \end{aligned} \tag{2.33}$$

II.4.c. Numerical results

The analytical procedure so far followed, can be validated by comparing the sequence $i_s(n,0)$ with the one given by a numerical solution. The transient due to the sudden connection of the active filter in parallel to the network has been considered for such a comparison. Assuming that all initial conditions are nil, $\varphi = -\pi/6$, $r_s = 10 \Omega$, $l_s = 5 \text{ mH}$, $C = 1 \text{ mF}$, the results are shown in fig.2.9, where the solid line represents the current in a phase of the filter obtained by means of a numerical integration and the dots are the values of the sequence $i_{s1}(n,0)$ evaluated by performing the inverse z-transform.

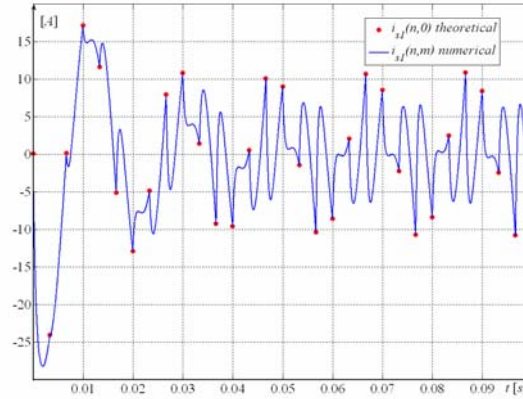


Fig.2.9. Comparison between analytical and numerical initial values of y_i .

In the next figs.2.10 it can be observed the surfaces depicted by y_{rss} and y_{iss} as a function of α and β when $r_s = 1 \Omega$ and $\varphi = 0$. It can be seen for both y_{rss} and y_{iss} that the dependence on β is negligible when β is greater than 10^{-4} s. The numerical analysis carried out has pointed out that value

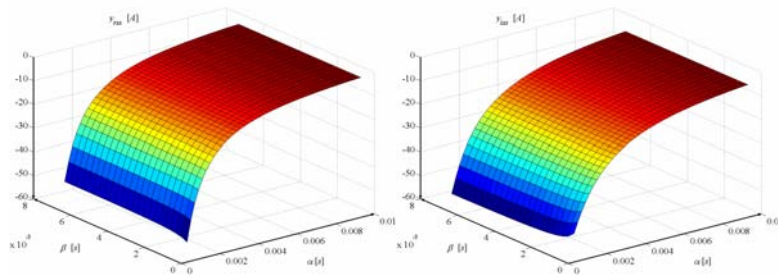


Fig.2.10. Steady-state values of y_r and y_i as a function of the inner parameters of the filter

of r_s is only a multiplying factor for the previous surfaces. A further numerical investigation leads to the evaluation of the dependence of the steady-state values of y_{rss} and y_{iss} on the filter inner parameters r_s , l_s and C . This is shown in

fig.2.11 for the sequence y_{rSS} .

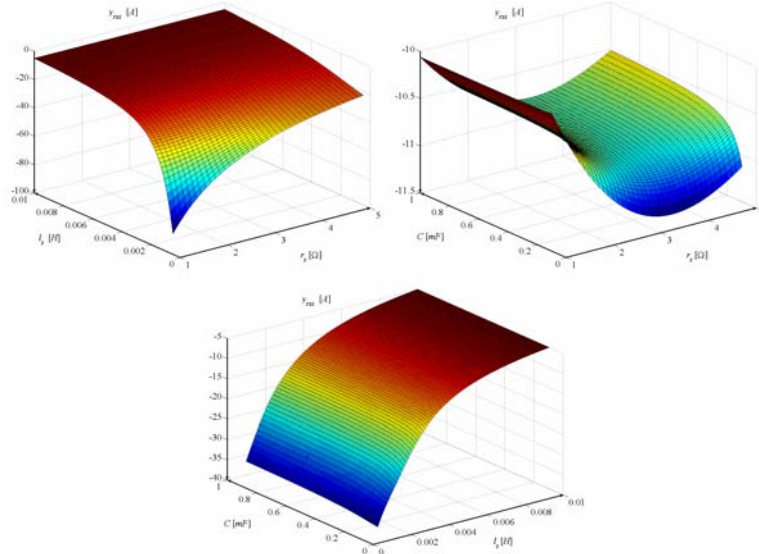


Fig.2.11. Dependence on inner filter parameters of steady-state values of y_{rSS}

The analysis of the figures highlights that the dependence on C is in practice negligible if C is greater than 0.1 mF. In addition, for values of inductance l_s greater than 5 mH, the dependence on r_s is also very small. This means that if l_s is large enough it is possible to obtain the same filter performances with a very small resistance. In practice this is realised using a pure inductive filter, whose resistance is that of the winding around the magnetic core.

From relations (2.32) it is easy to obtain the steady-state expression of the current i_s :

$$\tilde{i}_s(m,n) = (\tilde{y}_r + j\tilde{y}_i) e^{j\frac{\pi}{3}n} \quad (2.34)$$

In fig.2.12 the steady-state current waveforms in a phase calculated by means of the analytical method and of a numerical integration are compared when $l_s = 5$ mH, $r_s = 10$ Ω, $C = 1$ mF, $\varphi = 0$. The relative error between the numerical solution and the analytical solution is about 0.5%. The error in the numerical solution is due to the maximum tolerance assigned for the integration of the system. It has been verified indeed that using a smaller tolerance the waveform given by the numerical solution is closer to the analytical solution. This aspect point out the advantage of an analytical solution in terms of the amount of time saved for the integration of the mathematical model of the system.

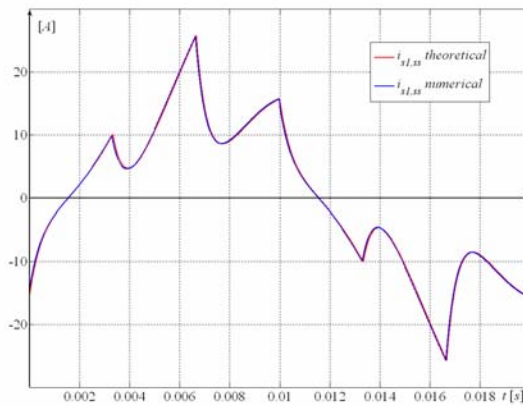


Fig.2.12. Comparison among analytical and numerical solution

A further numerical investigation makes it possible to evaluate the dependence of some quantities of interest not only on inner filter parameters, e.g. r_s , l_s and C , but also on the filter control parameter φ . This is shown in figs.2.13 for the rms value of the filter current, $I_{s,rms}$. The figures highlight that the value of φ allow the control of the rms

value in a wide range. The minimum of $I_{s,rms}$ is reached when the first harmonic of the inverter output voltage is in phase with the network voltage, occurring when φ is equal approximately to -30° . In addition, $I_{s,rms}$ is in practice independent on C and also the dependence on I_s is not remarkable. Conversely, the dependence on r_s is very strong especially when the resistance is less than 5Ω .

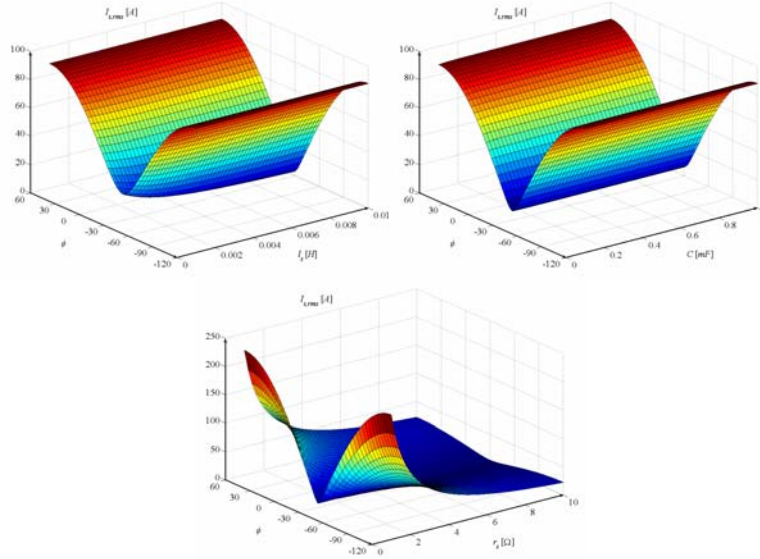


Fig.2. 13. Dependence on inner filter parameters of the rms value of the current

II.4.d. Harmonic analysis

From the analysis of fig.2.12, it could be interesting to investigate into the variation of the current harmonics with the phase angle φ of the space vector of the supplied voltage. Expressing the steady-state current \tilde{i}_s by the Fourier complex expansion:

$$\tilde{i}_s = \sum_{\nu=-\infty}^{+\infty} i_{s\nu} e^{j\nu \frac{2\pi}{T} t},$$

the coefficients $i_{s\nu}$ can be calculated in the following way:

$$i_{s\nu} = \frac{1}{T} \int_0^T \tilde{i}_s e^{-j\nu \frac{2\pi}{T} t} dt = \frac{1}{T} \sum_{n=0}^5 \int_{\frac{nT}{6}}^{\frac{(n+1)T}{6}} \tilde{i}_s e^{-j\nu \frac{2\pi}{T} t} dt. \quad (2.35)$$

Performing the change of variables:

$$t = (n+m) \frac{T}{6},$$

and taking into account the equation (2.34), the coefficients (2.35) can be rewritten as follows:

$$\begin{aligned}
 i_{sv} &= \frac{1}{6} \sum_{n=0}^5 \int_0^1 \tilde{y}(m) e^{j\frac{\pi}{3}n} e^{-j\frac{\pi}{3}(n+m)v} dm = \\
 &= \frac{1}{6} \frac{1 - e^{j\frac{5\pi}{3}(1-v)}}{1 - e^{j\frac{\pi}{3}(1-v)}} \int_0^1 \tilde{y}(m) e^{-j\frac{\pi}{3}mv} dm
 \end{aligned}
 \tag{2.36}$$

In the following fig.2.14, the harmonic content of the current is reported for different values of the phase angle φ . The analysis of the figures shows that the harmonic distribution is almost the same except for $\varphi = -30^\circ$, where the current assumes very low values. These considerations demonstrate that such a structure, controlled by square-wave voltages, cannot be usefully adopted as a selective harmonic filter, because it does not make it possible to inject desired current harmonics into the network. However, the I^{st} harmonic current amplitude changes remarkably with the phase angle φ and then the square-wave control allows the active filter to compensate the reactive power.

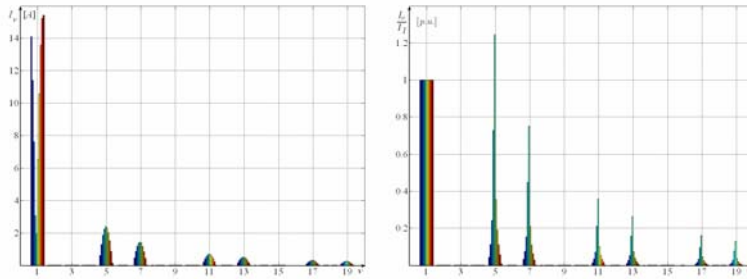


Fig.2.14. Harmonic analysis for different values of phase angle φ

II.5. CONCLUSIONS

The chapter has shown that it is possible to achieve a closed form solution for the mathematical model of shunt active filters. Difficulties arising from the non-linearity of the model has been overcome by a proper use of the modified z -transform. Due to the non-linearity of the mathematical model, the analytical solution has been determined only by referring to square-wave operations. In particular, the sampling period has to be chosen equal to the switching frequency. The solution obtained is very useful to get analytical expressions of current harmonics generated by filters and to evaluate their reactive power compensation. Cause the complexity of the calculus procedure followed, the solution has been numerically validated, in order to verify both the correctness and the accuracy.

III

DIMENSIONING PROCEDURE OF THE PASSIVE ELEMENTS OF AN ACTIVE FILTER

III.1. INTRODUCTION

The design of physical systems mainly consists in the evaluation of inner parameter values, which obtain required outputs for given inputs. This target is in general achieved using relationships among system inputs and outputs. These relationships represent mathematical models of physical systems and are usually expressed by means of sets of algebraic and/or differential equations. The functions representing inputs and outputs are related one to the others by algebraic operations involving the characteristic parameters of the system. Mathematical models can be successfully used for the evaluation of design algorithms, if their sets of equations are rearranged and solved by considering unknown the inner parameter values and known both the inputs and the outputs. Unfortunately, this calculus procedure is sometimes difficult, because some sets of equations of the mathematical models do not immediately give rise to solutions expressed in closed analytical forms. Alternatively, “put and try” design procedures are, hence, used [12]. Such procedures mainly consist of the selection of a “first attempt” set of values of system inner parameters and of the solution of the system mathematical model aiming to evaluate output functions and to verify whether these approach the expected ones in a given time interval. If this is not, a suitable modification of former parameter values is required. The procedure must be iterated until output functions approach the expected ones with the required design accuracy. This design procedure obviously requires great deal of calculus time and seldom obtains final parameter values that satisfy optimised conditions.

Design procedures of power electronics devices are the same of all physical systems, because their design implies:

- the correct choice of passive components (i.e. resistances, inductances and capacitor values);
- the most suitable control laws of power semiconductors (i.e. the evaluation of a digital program which states conducting and non-conducting time intervals).

At the state of the art, the mathematical model of active filters is represented by a set of non-linear differential equations and its definition requires the use of generalised function theory. As the previous chapter has underlined, the mathematical model can be solved by using integral transformations and the solutions are expressed in closed analytical forms. The suggested analytical solution can be useful for different reasons. It offers the opportunity to evaluate simple design guidelines which are also able to satisfy given optimal boundary conditions.

The extensive use of power electronics devices will lead to a reduction in their costs and will therefore also provide small power plants with active filters. To encourage their widespread use, it might be convenient to design devices whose performances are optimised with reference to single plant requirements and whose costs are the lowest possible ones. The chapter shows how these results can be achieved practically by means of previous theoretical results. A numerical example, optimising the filter cost with respect to its performances, is suggested and a reference table for optimised values of filter parameters as a function of p.u. filter reactive power is given.

III.2. APPLICATION TO THE DESIGN GUIDELINES

The analytical solution which has been found for filter currents is represented by relationships expressed by means of well-known exponential and trigonometric functions. At steady-state these functions are algebraically related to inner parameter values of the filter. Therefore, they reveal some interesting properties of filter behaviour and, in particular, how the filter parameters affect the current waveform. It is interesting to notice that parameters l_s , r_s , C appear in the solution not alone, but combined as:

$$\alpha = \frac{l_s}{r_s}$$

$$\beta = \frac{3}{2} r_s C$$

Unknown filter current amplitudes are, besides, proportionally direct to supplied network voltage amplitude. In particular, it affects current only by means of V_s / l_s and active and reactive powers by means of V_s^2 / l_s . The found analytical solution shows that only the quantities α , β , V_s / l_s and the phase angle φ between network and square wave voltages influence filter behaviour. This means that it is immediately possible to know how the filter parameters and filter control law separately influence filter behaviour.

Since V_s / l_s is only a multiplying factor, steady-state filter behaviour can be simply analysed by assuming $V_s / l_s = 1$ and scaling properly design results. According to previous considerations reference is made to mean values of scaled reactive and active powers, i.e.:

$$\gamma = \frac{Q l_s}{V_s^2}; \lambda = \frac{P l_s}{V_s^2}$$

The compensation of the reactive power is a first goal that active filters have to achieve. Therefore, it would be interesting to analyse how this can be obtained selecting filter parameters by means of the solution found for filter currents. Moreover, the analytical expression found for the filter currents does not make a weight-analysis of the influence of filter parameters on reactive power immediately possible, because the relationships among this power and combined filter parameters are themselves non-linear. A numerical approach to the problem is, therefore, more useful because it is easy to evaluate the reactive power and the power factor $\cos\psi = \cos[\tan^{-1}(\gamma / \lambda)]$ as a function of α and φ . In particular, these quantities can be represented by the surfaces shown in fig.3.1a and fig.3.1b respectively in the spaces $(\alpha, \varphi, \gamma)$ and $(\alpha, \varphi, \tan\psi)$. Projecting the surface of fig.3.1b, representing $\tan\psi$, in the plane $(\tan\psi, \varphi)$, fig.3.2a is obtained. Finally, fig.3.1c gives the rms values of the scaled filter current, $I_{s,rms,pu}$, which is the current obtained with the voltage of 1 V and an inductance of 1 H.

For a fixed value of the power factor and, hence, of $\tan\psi$ and for each value of α , it is possible to evaluate the value of φ . Each pair (α, φ) also yields the evaluation of γ , as fig.3.1a shows. Therefore it is possible to draw a diagram $\gamma = \gamma(\alpha)$ for different $\tan\psi$ (see fig.3.2b). As a further numerical investigation demonstrates, for different power factors the scaled reactive power γ is approximately a linear function of α in a wide range. The results are very useful in practice because, for a fixed value of output reactive power, they also make it possible to easily carry out an analytical expression, which relates r_s and l_s for different $\tan\psi$. This is shown in fig.3.3 in the sample case of $Q = 10 \text{ kVAR}$.

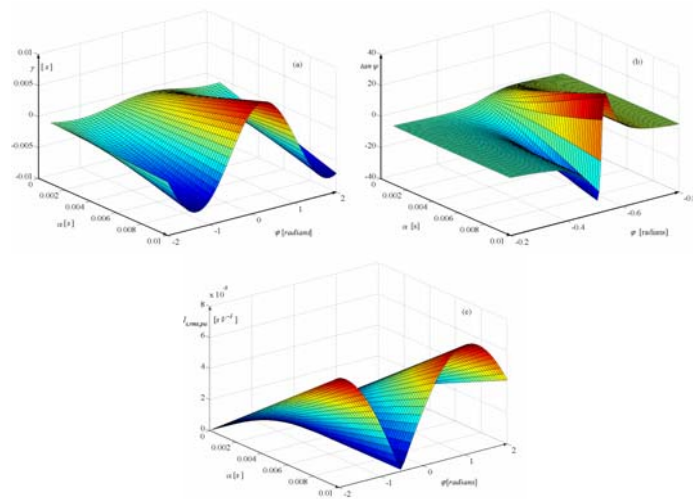


Fig.3.1. Scaled reactive power (1a), $\tan \psi$ (1b) and $I_{s,rms,pu}$ (1c) as a function of α and φ

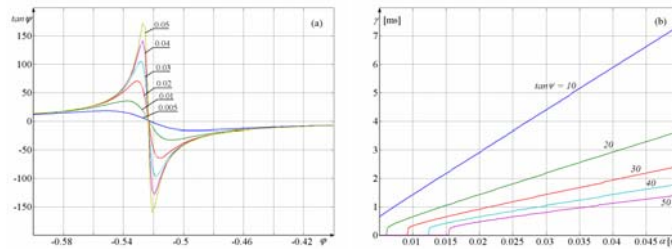


Fig.3.2. The ratio $\tan \psi$ as a function of φ for different values of α (2a) and scaled reactive power as a function of α for different values of $\tan \psi$ (2b)

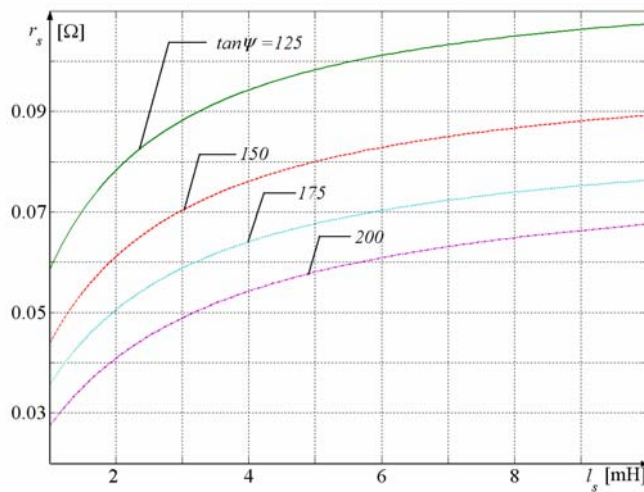


Fig.3.3. Related resistance and inductance values, that give rise to different $\tan \psi$ values

III.3. SAMPLE DIMENSIONING WITH NUMERICAL VERIFICATION

In order to explain and to verify the suggested dimensioning procedure, a numerical example has been taken into consideration. It is supposed that the reactive power to be compensated is $Q = 10$ kVar and the network voltage is 220 V rms with frequency equal to 50 Hz.

A first attempt value of the inductance l_s can be selected in the range of typical applications of active filters, for example 5 mH. Therefore, the scaled reactive power can be evaluated:

$$\gamma = \frac{Q l_s}{V_s^2} = 5.16 \cdot 10^{-4} \text{ s} .$$

In order to keep the losses negligible respect to the reactive power exchanged, $\tan \psi$ should be selected very high. Choosing $\tan \psi = 40$ and reminding the value of γ previously evaluated, the value of α is given by fig.3.2b and it is:

$$\alpha = 0.017 \text{ s} .$$

The value of α , associated with the first attempt value of I_s , yields the filter resistance r_s :

$$r_s = \frac{I_s}{\alpha} = 0.29 \Omega .$$

The dimensioning procedure need to be completed by the evaluation of the rated current of the filter for the selected reactive power. Fig.3.2a gives the value of the phase shift φ for the selected values of α and $\tan \psi$.

$$\varphi = -0.503 .$$

Finally, fig.3.1c gives the corresponding rms value of the current:

$$I_{s,rms} = 16.71 \text{ A} .$$

The diagrams of the network voltage and of the filter ac side current have been shown in the fig.3.4 in the examined conditions.

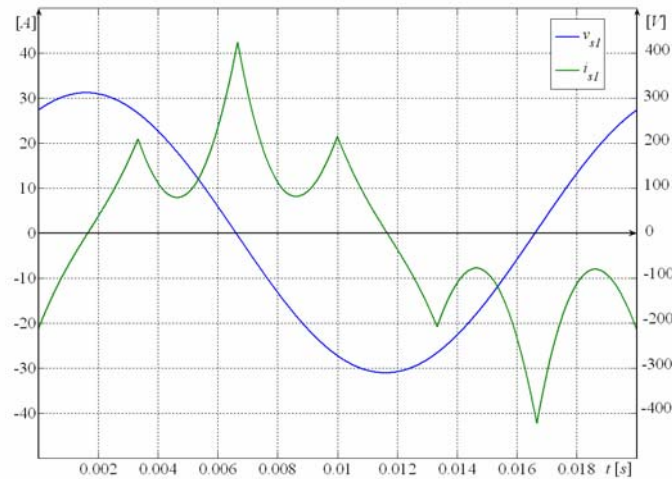


Fig.3.4. Voltage and current waveforms for the considered example

The numerical verification of filter behaviour, in the case of the inner parameter are evaluated following the suggested criterion, yield there results:

- reactive power compensated:

$$Q = 9.93 \text{ kVAr} ;$$

- power losses:

$$P = 246 \text{ W} ;$$

- power factor:

$$\cos \psi = \cos \left[\tan^{-1} \left(\frac{Q}{P} \right) \right] = 0.025 ;$$

- rms current on the ac side:

$$I_{s,rms} = 16.71 \text{ A} .$$

III.4. COST OPTIMIZATION FOR THE INDUCTIVE FILTER DESIGN

Fig.3.3 gives evidence that there are many different pairs of filter resistance and inductance values leading to the same operating conditions. The result suggests to investigate whether the choice of passive elements of filter structure can be optimised with reference to a given condition. A criterion chosen for the optimisation may be the lowest cost of the copper needed for inductance because, if the cost of the core and the shell is neglected, the lowest cost of the filter is implied by the minimum copper volume.

Reference is made to a shell-type ferromagnetic core (see fig.3.5). The following geometric expressions of the magnetic lengths of yokes and columns can be obtained:

$$h_y = l_w + \Delta' + R ;$$

$$h_c = h_w + 2\Delta .$$

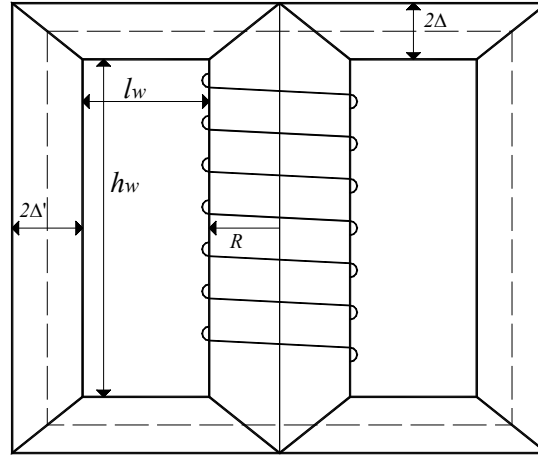


Fig.3.5. Schematic representation of the inductance structure

Previous relationships immediately lead to express resistance and inductance values as a functions of geometrical dimensions. Assuming that all N turns are wound around the central column and the winding is built by n layers each made by n_s turns in series, there results:

$$\begin{aligned} r_s &= \sum_{i=0}^{n-1} \sum_{j=1}^{n_s} \frac{2\pi\rho}{ab} \left[R + \left(\frac{a}{2} + ia \right) \zeta_{cu} \right] = \\ &= \frac{2\pi\rho}{ab} n n_s \left(R + \frac{a}{2} n \zeta_{cu} \right) \end{aligned}$$

where $\zeta_{cu} \geq 1$ takes into account the thickness of electrical insulation. Since $n \cdot n_s = N$, $a \cdot b = S_{cu}$ and $\zeta_{cu} \cdot a \cdot n \cong l_w$, the previous equation yields:

$$r_s \cong \frac{\pi\rho}{S_{cu}} N (2R + l_w). \quad (3.1)$$

However, the winding cannot fill the window of ferromagnetic core completely, because the shape of the conductors implies that the total copper area is less than the window area. By taking into account the copper space factor, ε_f it can be written:

$$N S_{cu} \varepsilon_f = l_w h_w .$$

For the evaluation of the inductance it has been supposed that the magnetic field lines link the whole winding:

$$l_s = \frac{N^2}{\frac{h_y}{\mu_y S_y} + \frac{h_c}{2\mu_c S'_c} + \frac{h_c}{\mu_c S_c}}$$

By taking into account that $S'_c = S_c / 2$ and $S_y / S'_c = \Delta / \Delta'$, the previous equation yields:

$$l_s = \frac{\mu_c N^2 \frac{\pi R^2}{2}}{h_w + 2\Delta + \frac{\mu_c}{\mu_y} \frac{\Delta'}{\Delta} (l_w + \Delta' + R)} \quad (3.2)$$

The copper volume needed by the winding is, hence, finally given by:

$$V_{cu} = N l_m S_{cu} = \frac{l_s S_{cu}^2 \varepsilon_f}{2\mu_c} \frac{l_w + 2R}{l_w R^2} \left\{ I + \sqrt{I + \frac{2\mu_c \pi l_w^2 R^2}{l_s S_{cu}^2 \varepsilon_f^2} \left[2\Delta + \frac{\mu_c}{\mu_y} \frac{\Delta'}{\Delta} (l_w + \Delta' + R) \right]} \right\} \quad (3.3)$$

In order to reduce iron losses and the reactive power of ferromagnetic cores, the ratio S_y / S'_c is generally equal to 1.15, up to 1.2 [13]. In the case under consideration it has been set $\Delta / \Delta' = 1.2$. Eq. (3.3) expresses the copper volume as a function not only of geometrical dimensions, i.e. l_w , S_{cu} , R , Δ , but also of filter inductance l_s . However, the section of copper wire S_{cu} may be considered as a given value, because it depends on the rated current of the filter. Therefore, the value of S_{cu} has been chosen well-matched with the reactive power to be compensated and with the desired power factor. Then, after the dimensioning the *rms* current has to agree with the selected copper section. Eq. (3.3) shows indeed that, for a fixed value of the ratio Δ / Δ' , the copper volume is an increasing function of Δ and, hence, the minimum belongs to the boundary. The value of Δ can be chosen as equal to those traditionally used in the construction of inductors, i.e. 2-3 cm. Finally, for each given value of inductance l_s , it is possible to draw a surface of the volume as a function of the column radius R and the window length l_w , as fig. 3.6 shows. From eq. (3.3) the minimum of copper volume with respect to variables R and l_w can be evaluated. The analytical evaluation of this minimum is not simple, because it implies the calculus of partial derivatives and the determinant of the Hessian matrix. However, it is more suitable to evaluate the relative minimum of the function using a numeric procedure. The minimisation procedure can be performed for different values of inductance l_s . The influence of the inductance value on geometric dimensions of the inductor is shown in fig.3.7.

The suggested procedure requires a preliminary choice of the inductance l_s , whose value yields the evaluation of the resistance, r_s , the number of turns, N , the window length, l_w , and the column radius, R . Therefore, a further calculus step can lead to the evaluation of a more general optimal solution. Among different inductance values, hence, the most appropriate one can be selected in order to satisfy an auxiliary condition useful for satisfying given filter ratings. For this reason, it can be considered that each pair of filter inductance and resistance values

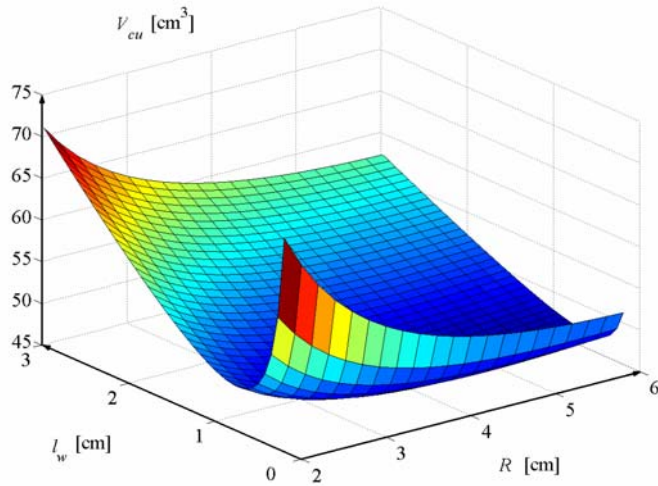


Fig.3.6. Winding copper volume as a function of R and l_w

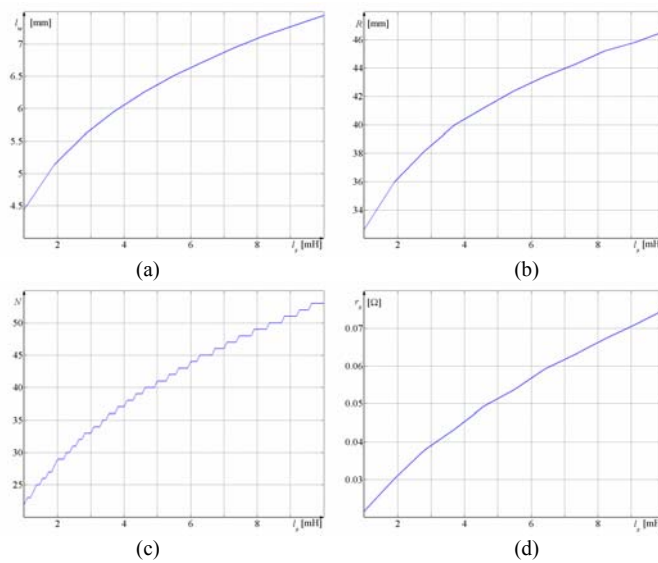


Fig.3.7. Geometric quantities of filter as a function of inductance l_s

defines a value of $\tan\psi$ (see fig.3.3). Therefore the function $\tan\psi = \tan\psi(r_s, l_s)$ can be represented by a surface in the space $(r_s, l_s, \tan\psi)$. On the other hand, as fig.3.7d shows, the criterion of the minimum cost gives a functional relationship between r_s and l_s . Therefore only geometrical quantities are involved. The relation is not dependent on the value of $\tan\psi$ and, then, it is represented as a cylindrical surface in the space $(r_s, l_s, \tan\psi)$, as fig.3.9 shows. The curve obtained from the intersection of these two surfaces can be projected both in the plane $(\tan\psi, r_s)$ and in the plane $(\tan\psi, l_s)$ yielding the curves $r_s = r_s(\tan\psi)$ and $l_s = l_s(\tan\psi)$. Finally, the inductance and the resistance, which satisfy both filter ratings and minimum cost design can be evaluated for each $\tan\psi$ value. This is shown in fig.3.10. As an example (see Tab.3.I), the dimensions of the inductance have been carried out.

Tab.3.I. Sample design of core shapes using the minimisation procedure proposed

		r_s	$l_{w,min}$	R_{min}	h_y	h_w	N	B_c
		[Ω]	[mm]	[mm]	[mm]	[mm]		[T]
l_s [mH]	5	0.05	6.5	42	65	19	40	1.13
μ_c	100							
Δ [cm]	2							

III.5. CONCLUSIONS

The chapter has presented a design criterion of active filter hardware for the choice of main electrical parameter values, i.e. of r_s , l_s and C . The evaluation of these values has been made according to the expected performances of the filter and the minimum cost of core inductance. The analytical solution of the non-linear system of equations representing the mathematical model of active filters when they operate with square-waves has been written making use of integral transformations. It has been possible, hence, to select inner filter parameters that satisfy given

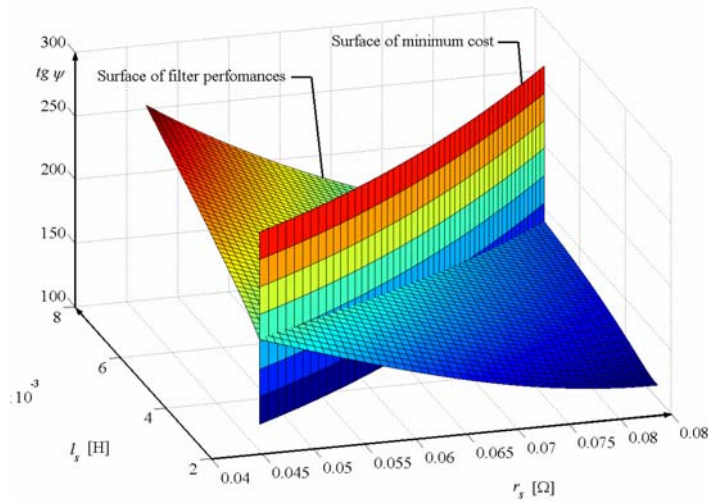


Fig.3.8. Intersection between the surface of optimal geometric dimensions and the surface of requested filter performances

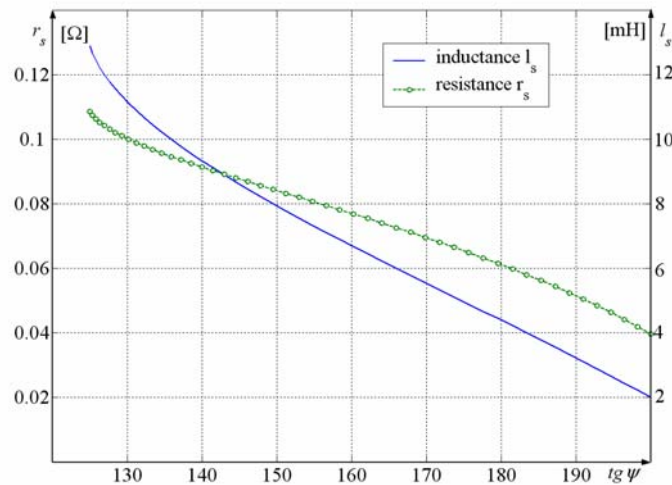


Fig.9. Resistance and inductance values obtained from the minimum cost criterion as a function of $tg \psi$

performances. The analytical procedure has been explained and diagrams that can be successfully used as guidelines for active filter design has been shown.

IV

CONTROL TECHNIQUES OF ACTIVE FILTERS USED FOR HARMONIC COMPENSATION

IV.1. INTRODUCTION

The other aspect of the analysis of mathematical models of physical systems is the resolution of inverse problems, i.e. the evaluation of the input to be applied for obtaining desired outputs. The study implies that unknown quantities, e.g. the currents in an electric circuit, have to be considered known whereas inputs are the unknown quantities to be evaluated by the resolution of the mathematical model.

A large technical literature, until now published, has dealt with the analysis of the most profitable control technique of active filters and with the problems of harmonic detection of current generated by non-linear loads. Most active power filters are controlled on the basis of the instantaneous reactive power theory, introduced by Akagi and Nabae [9]. The phase voltages and currents are transformed into a reference frame with the axis α and β . The instantaneous real power, $p(t)$, supplied to load and the instantaneous imaginary power, $q(t)$, are then calculated in this representation system. However, there is a one-to-one correspondence between the α and β components and the voltage and currents in the three phases. The powers $p(t)$ and $q(t)$ can be, hence, expressed directly as functions of voltages and currents in the three phases without the transformation in the α and β frame. In case of symmetrical supply voltages and balanced load currents, the instantaneous power and the instantaneous reactive power are constant. If the active filter control is able to hold constant these two quantities, the currents flowing in the load are forced to be sinusoidal and balanced. In addition, the compensation of the reactive power is achieved by putting $q(t) = 0$. The expression of the reference compensating currents can be obtained, hence, from the values of $p(t)$ and $q(t)$. The reference current signals and the detected output currents of active filter can be thus sent to a current controller to generate the pulse width modulation (PWM) signals required for the operation of control circuits. Nevertheless, if the supply voltages are not sinusoidal, the use of the instantaneous reactive power theory leads to that the load currents are not sinusoidal even if the instantaneous powers $p(t)$ and $q(t)$ are constant. Therefore modifications and extensions of the original theory were introduced to overcome these disadvantages [15]. The line currents are sinusoidal, also in systems with non-sinusoidal supply voltages, if the reference currents supplied by the active filter are calculated starting from the first voltage harmonic of direct sequence instead of the whole supply voltages, as it was in the original theory.

Results obtained are, hence, useful to verify operating conditions but these are not fully satisfying for designing always the best control laws regarding a specific problem. An interesting practical problem to be solved consists, indeed, in the evaluation of active filter controlling laws, which really obtain the compensation of a given harmonic set. To solve this problem, it is necessary to know analytical relationships between harmonics generated by the filter and its control laws. By means of well-known mathematical operations, the system of differential equations representing the model of a shunt active filter has been solved using the methods explained in the chapter II. The solutions are expressed as exponential and trigonometric time functions dependent on filter characteristic

parameters. The resolution of the mathematical model gives useful guidelines for the evaluation of suitable control techniques with the aim to obtain the desired output in terms of reactive power and harmonic content of currents.

A feeding algorithm for compensating the reactive power required by the load and the harmonic currents is presented in this chapter. The algorithm is valid in general, even if unsymmetrical voltages and unbalanced currents are involved. The output of the feeding algorithm is the space vector of the voltage supplied by the inverter, which is the reference voltage for the Space Vector Modulation. Numerical simulations compare the results obtained from an ideal inverter capable of supplying the reference space vector of voltage with those obtained from theoretical results.

IV.2. FEEDING ALGORITHM USED FOR HARMONIC COMPENSATION

For sake of simplicity reference has been made to the ideal filter configuration represented by the equivalent electrical network of fig.4.1. The filter operates as a shunt active filter. In the analysis, the switches are considered ideal and the commutations instantaneous. Therefore, the circuit configuration of fig.4.1 can be represented by the following system of non-linear differential equations:

$$\begin{cases} \mathbf{v}_s + r_f \mathbf{i}_f + l_f \frac{d\mathbf{i}_f}{dt} = \frac{2}{3} v_{dc} \zeta(t) e^{j\eta(t)} ; \\ \frac{dv_{dc}}{dt} = -\frac{1}{C} \text{Re}\{\mathbf{i}_f \zeta(t) e^{-j\eta(t)}\}. \end{cases} \quad (4.1)$$

The evaluation of a feeding algorithm for harmonic compensation requires the determination of inverter inputs which obtain desired currents. This can be achieved by the inversion of the mathematical model considering as inputs the space vector of current \mathbf{i}_f and as unknown quantities the functions $\zeta(t)$ and $\eta(t)$, expressing the inverter control law. Generally, the solution of this problem yields continuous time functions which cannot be obtained in a real inverter. Therefore, this solution can be used in practice only as reference input for the Space Vector Modulation, which provide to realise actual inverter voltages with a good approximation respect to desired voltages.

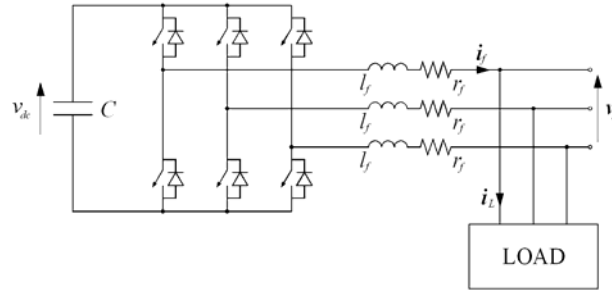


Fig.4.1. Equivalent electrical network of a sample configuration of a shunt active filter

Solving for $\zeta(t)$ and $\eta(t)$ the mathematical model expressed by the system of eqs. (4.1), it is possible to write the following three equations:

$$\begin{cases} e^{j\eta(t)} = \frac{\left(\mathbf{v}_s + r_f \mathbf{i}_f + l_f \frac{d}{dt} \mathbf{i}_f \right)}{\left| \mathbf{v}_s + r_f \mathbf{i}_f + l_f \frac{d}{dt} \mathbf{i}_f \right|}, \\ \frac{2}{3} \xi(t) v_{dc} = \left| \mathbf{v}_s + r_f \mathbf{i}_f + l_f \frac{d}{dt} \mathbf{i}_f \right|, \\ \frac{d}{dt} v_{dc}^2 = -\frac{3}{C} \left[\operatorname{Re} \left\{ \mathbf{v}_s \mathbf{i}_f \right\} + r_f I_f^2 + l_f \frac{d}{dt} I_f^2 \right]. \end{cases} \quad (4.2)$$

Two of these equations are algebraic and one differential, where the dc side voltage v_{dc} is involved. It is easily seen that in the system of eqs. (4.2) there are three equations in five unknown quantities, i.e. $\xi(t)$, $\eta(t)$, $\operatorname{Re}(\mathbf{i}_f)$, $\operatorname{Im}(\mathbf{i}_f)$ and $v_{dc}(t)$. In order to solve univocally the system of eqs. (4.2), two auxiliary conditions are needed. For that reason, it is possible to assign arbitrarily the real and imaginary component of \mathbf{i}_f . Fixed the desired current space vector, the inverter control law, given by both the functions $\{\xi(t), \eta(t)\}$, is evaluated. Although the space vector \mathbf{i}_f is the input of system (4.2), it is also possible to held constant the mean value of dc voltage, v_{dc} . In other words, this means that v_{dc} is a periodic function. Therefore, the real and imaginary parts of \mathbf{i}_f are no more arbitrarily assigned, but they have to satisfy the following equation:

$$\frac{1}{T} \int_0^T v_{dc} \frac{d}{dt} v_{dc} dt = -\frac{3}{2CT} \int_0^T \left[\operatorname{Re} \left\{ \mathbf{v}_s \mathbf{i}_f \right\} + r_f I_f^2 + l_f \frac{d}{dt} I_f^2 \right] dt. \quad (4.3)$$

The first integral is identically nil, because v_{dc} is supposed to be a periodic function and, hence, $v_{dc}(T) = v_{dc}(0)$. Eq. (4.3) yields, then:

$$\int_0^T \left[\operatorname{Re} \left\{ \mathbf{v}_s \mathbf{i}_f \right\} + r_f I_f^2 \right] dt + l_f \left[I_f^2(T) - I_f^2(0) \right] = 0. \quad (4.4)$$

IV.2.a. Feeding algorithm used for harmonic compensation

It is clear that the feeding algorithm expressed by eqs. (4.2) with the auxiliary condition given by eq. (4.4) is valid in general, for every main voltages and desired filter currents, since instantaneous space vectors are involved. This means that the algorithm allows the active filter to compensate both the load reactive power, the current harmonics and the load unbalance, e.g. due to different resistances and inductances of each phase and to the distortion of mains voltages. Although the solution can be expressed in analytical closed form for every voltages \mathbf{v}_s and currents \mathbf{i}_f , the calculation of the integrals involved is possible only in particular cases. One of this is the very interesting case of steady-state operations and periodic solutions. In these hypothesis, it is possible to write the output current of inverter \mathbf{i}_f by means of its Fourier expansion, i.e.:

$$\mathbf{i}_f(t) = \sum_{v=-\infty}^{+\infty} \mathbf{I}_{f,v} e^{jv\omega t}.$$

Stating this expression of \mathbf{i}_f , from eq. (4.4) it is:

$$I_f^2(t) = \left(\sum_{k=-\infty}^{+\infty} I_{f,k} e^{jk\omega t} \right) \left(\sum_{v=-\infty}^{+\infty} I_{f,v} e^{-jv\omega t} \right) = \sum_{k=-\infty}^{+\infty} \left(\sum_{v=-\infty}^{+\infty} I_{f,v} I_{f,v-k} \right) e^{jk\omega t} ;$$

$$I_f^2(T) = I_f^2(0) = \sum_{k=-\infty}^{+\infty} \sum_{v=-\infty}^{+\infty} I_{f,v} I_{f,v-k} .$$

Moreover, sinusoidal voltages yield:

$$v_s = V_s e^{j\omega t} ,$$

and, then, eq. (4.4) becomes an algebraic equation:

$$V_s^R I_{f,l}^R + V_s^I I_{f,l}^I + r_f \sum_{v=-\infty}^{+\infty} |I_{f,v}|^2 = 0 . \quad (4.5)$$

Rearranging eq. (4.5) it can be written:

$$r_f (I_{f,l}^R)^2 + V_s^R I_{f,l}^R + V_s^I I_{f,l}^I + r_f (I_{f,l}^I)^2 + r_f \sum_{\substack{v=-\infty \\ v \neq l}}^{+\infty} |I_{f,v}|^2 = 0 \quad (4.6)$$

Eq. (4.6) puts in evidence that it is also possible to control the reactive power flowing between the active filter and the load, since the imaginary part of the first harmonic can be selected arbitrarily. This means that the power factor of the load can be reduced to the unity. Therefore, solving for the real part of first harmonic of i_f , it is:

$$I_{f,l}^R = -\frac{V_s^R}{2r_f} \pm \sqrt{\left(\frac{V_s^R}{2r_f} \right)^2 - \frac{V_s^I I_{f,l}^I}{r_f} - (I_{f,l}^I)^2 - \sum_{\substack{v=-\infty \\ v \neq l}}^{+\infty} |I_{f,v}|^2} . \quad (4.7)$$

If the first harmonic of the space vector i_f is selected so that the eq. (4.7) is satisfied, the active filter control yields dc side voltages v_{dc} with constant mean value. The integration of the third of eqs. (4.2) gives the expression of v_{dc} as function of the time:

$$v_{dc}^2(t) - v_{dc}^2(0) = -\frac{3}{C} \int_0^t [\text{Re}\{\dot{v}_s i_f\} + r_f I_f^2] dt - \frac{3l_f}{C} [I_f^2(t) - I_f^2(0)] . \quad (4.8)$$

Moreover, the two integrals in eq. (4.8) can be analytically solved:

$$\int_0^t \text{Re}\{\dot{v}_s i_f\} dt = \text{Re} \left\{ \int_0^t \dot{v}_s \sum_{k=-\infty}^{+\infty} I_{f,k} e^{j(k-l)\omega t} dt \right\} =$$

$$= \text{Re} \left\{ \dot{v}_s I_{f,l} t + \sum_{\substack{k=-\infty \\ k \neq l}}^{+\infty} \frac{\dot{v}_s I_{f,k}}{j(k-l)\omega} [e^{j(k-l)\omega t} - 1] \right\} \quad (4.9)$$

$$\int_0^t r_f I_f^2 dt = \int_0^t r_f \left(\sum_{k=-\infty}^{+\infty} I_{f,k} e^{jk\omega t} \right) \left(\sum_{v=-\infty}^{+\infty} I_{f,v} e^{-jv\omega t} \right) dt =$$

$$= \int_0^t r_f \left[\sum_{k=-\infty}^{+\infty} \left(\sum_{v=-\infty}^{+\infty} I_{f,v} I_{f,v-k} \right) e^{jk\omega t} \right] dt = \quad (4.10)$$

$$= r_f \left(\sum_{v=-\infty}^{+\infty} I_{f,v}^2 \right) t + r_f \sum_{\substack{k=-\infty \\ k \neq 0}}^{+\infty} \sum_{v=-\infty}^{+\infty} \frac{I_{f,v} I_{f,v-k}}{jk\omega} [e^{jk\omega t} - 1] .$$

and therefore eq. (4.8) becomes:

$$\begin{aligned}
 v_{dc}^2(t) - v_{dc}^2(0) = & -\frac{3}{C} \left\langle \operatorname{Re} \left\{ \left(\sum_{k=-\infty, k \neq 1}^{+\infty} \frac{\dot{V}_s I_{f,k}}{j(k-1)\omega} [e^{j(k-1)\omega t} - I] \right) + \right. \right. \\
 & \left. \left. + r_f \left(\sum_{v=-\infty}^{+\infty} I_{f,v}^2 \right) t + r_f \sum_{k=-\infty, k \neq 0}^{+\infty} \sum_{v=-\infty}^{+\infty} \frac{I_{f,v} I_{f,v-k}}{jk\omega} [e^{jk\omega t} - I] \right\} + \right. \\
 & \left. - \frac{3l_f}{C} [I_f^2(t) - I_f^2(0)] \right\rangle. \tag{4.11}
 \end{aligned}$$

and reminding eq. (4.5):

$$\begin{aligned}
 v_{dc}^2(t) - v_{dc}^2(0) = & -\frac{3}{C} \operatorname{Re} \left\{ \sum_{k=-\infty, k \neq 1}^{+\infty} \frac{\dot{V}_s I_{f,k}}{j(k-1)\omega} [e^{j(k-1)\omega t} - I] \right\} + \\
 & - \frac{3r_f}{C} \sum_{k=-\infty, k \neq 0}^{+\infty} \sum_{v=-\infty}^{+\infty} \frac{I_{f,v} I_{f,v-k}}{jk\omega} [e^{jk\omega t} - I] - \frac{3l_f}{C} [I_f^2(t) - I_f^2(0)]. \tag{4.12}
 \end{aligned}$$

For the practical application of the proposed feeding algorithm to a real inverter can be used the block diagram shown in fig.4.2. The measured quantities are two line voltages and two load currents. By means of these currents, the DSP generates the voltage space vector and then the current harmonics. The detection of these harmonics is obtained by means of the

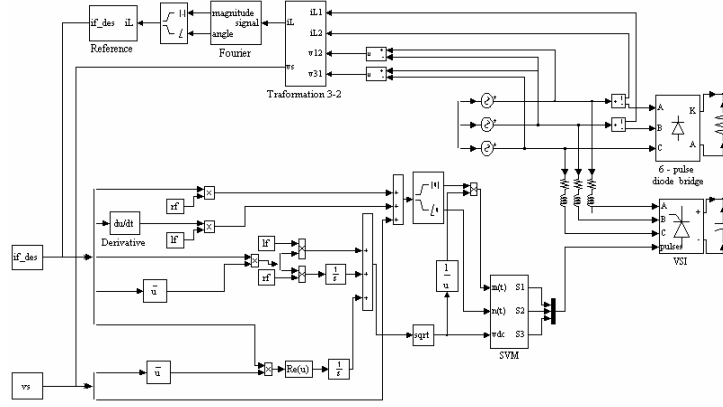


Fig.4.2. Block diagram of feeding algorithm for harmonic current compensation

Fast Fourier Transform (FFT) of the load current space vector. After the harmonic content has been identified, it is possible to select the current harmonics to be compensated. The compensation is obtained injecting the filter current harmonics, whose phase displacement is 180° shifted respect to load current harmonics. The integral and derivative operations given by eqs. (4.9) and (4.10) have been applied to input quantities, as fig.4.2 depicts, and finally the control signals $\{\xi(t), \eta(t)\}$ for the space vector modulation (SVM) have been obtained. The main advantage of this control algorithm is the analytical determination of inverter inputs for load harmonic compensation, obtained by the inversion of the ideal mathematical model of the filter. However, a problem which has to be solved so far is the real time identification of the harmonic content of load currents during transient conditions.

IV.2.b. Feeding algorithm used for load balancing

Another useful application of active filters is the load balancing. If an unbalanced sinusoidal load is considered,

it is easy to show that, assuming $\sum_{v=0}^2 i_v = 0$, the space vector of the current can be written as follows:

$$\mathbf{I}_L(t) = \mathbf{I}_{L,1} e^{j\omega t} + \mathbf{I}_{L,-1} e^{-j\omega t}.$$

The harmonic that the active filter has to compensate is then $I_{f,-1} = I_{L,-1}$. From eq. (4.8), there results:

$$\int_0^t \text{Re}\left\{ \mathbf{V}_s \mathbf{i}_f \right\} dt = \text{Re}\left\{ \mathbf{V}_s \mathbf{I}_{f,1} t - \frac{\mathbf{V}_s \mathbf{I}_{f,-1}}{2j\omega} (e^{-j2\omega t} - 1) \right\}; \quad (4.13)$$

$$\int_0^t r_f I_f^2 dt = r_f (I_{f,1}^2 + I_{f,-1}^2) t + 2 \text{Re}\left\{ \frac{\mathbf{I}_{f,1} \mathbf{I}_{f,-1}}{2j\omega} (e^{j2\omega t} - 1) \right\}. \quad (4.14)$$

As it has been previously shown, eq. (4.6) gives the real part of the first harmonic supplied by the filter. The compensation of the load reactive power involves the calculation of the value of the imaginary part of the first harmonic of the current.

IV.3. NUMERICAL RESULTS

The numerical results of the control algorithm can be easily verified by digital simulations of the whole system. It has been supposed to neglect the inner impedance of the line and the mains have been modelled as a three phase ac voltage source.

The main parameters of the inverter are given in Tab.4.I. Tab.4.II gives the parameter used for filter passive elements, i.e. r_f , l_f , C and the dc load r_u . The mains frequency, f , is 50 Hz, the maximum inverter switching frequency, f_s , is 10 kHz and the initial conditions taken into account are $I_{f0} = 0$ A and $v_{dc0} = 550$ V.

Tab.4.I. Main parameters of VSI

f_s [kHz]	S_n [kVA]	V_{dc} [V]
5	22	560

Tab.4.II. Parameters of filter passive elements and of load

r_f [Ω]	l_f [mH]	C [mF]	r_u [Ω]
0.5	5.0	1.65	25.9

The load is a six-pulse diode bridge connected in parallel with the shunt active filter, as shown in fig.4.1 The waveforms of load currents for an ideal six-pulse diode bridge are square-wave type. Their harmonic content can be expressed as follows:

$$I_{L,1+6k} = \frac{2\sqrt{3} I_d}{j\pi(1+6k)} \exp[-j(1+6k)\alpha] (-1)^k.$$

In the simulation, it has been supposed that the filter has to compensate only the 5th and 7th current harmonics, i.e. $I_{f,5} = I_{L,5}$ and $I_{f,7} = I_{L,7}$. Results of simulation are shown in figs. 4.3.

From fig.4.3a it can be noticed that the line current before the start-up of active filter has a strong harmonic content and the THD is 31.1%. After the filter control, the line current presents lower distortion. Its total harmonic distortion THD is indeed equal to 21.6%. Moreover, the control algorithm compensates the load reactive power realising an equivalent power factor equal to the unity, i.e. the phase angle between the first harmonic of the line current and the voltage line is nil. Fig.4.3b shows the real current of filter and the reference current. As it can be seen, the difference between the two currents is nil after few cycles. Fig.4.3c shows also that the voltage v_{dc} obtained from

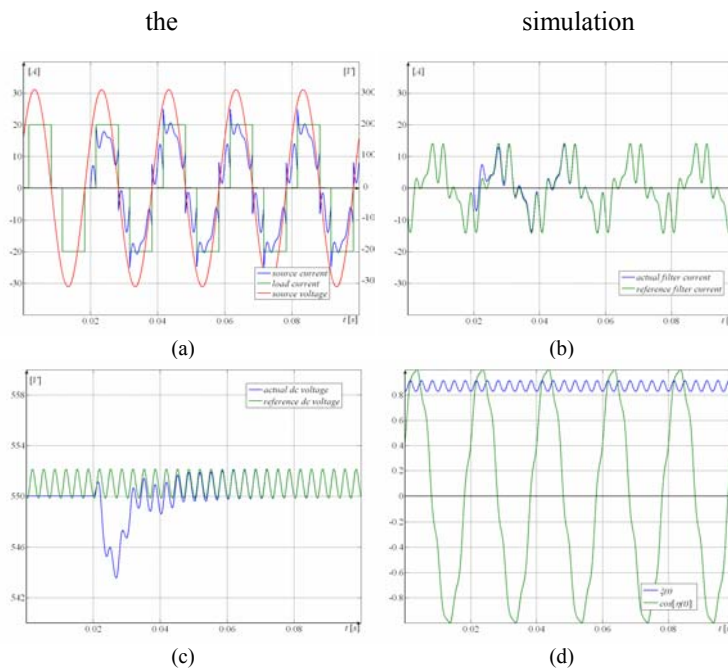


Fig.4.3. Digital simulation of harmonic compensation using the suggested algorithm

the numerically equal to the dc voltage evaluated in analytical way. In addition, the $\{\zeta(t), \eta(t)\}$ laws are shown in

fig.4.3d. The interaction among 1st, 5th and 7th harmonics gives rise to 6th and 12th harmonics in the spectrum of the control functions. Fig.4.4 shows the harmonic content of both the load current and the source current. From the figure it is evident that the active filter has been able to compensate the 5th and the 7th harmonics and the reactive power. Fig.4.4 shows indeed that also the first harmonic of the source current presents smaller amplitude than load current. This is confirmed by fig.4.3a where the current of the source is in phase with the voltage, whereas the same current of the load is lagging.

Another simulation has been carried out with the aim to compensate the unbalanced load, whose characteristics are shown in Tab.4.III.

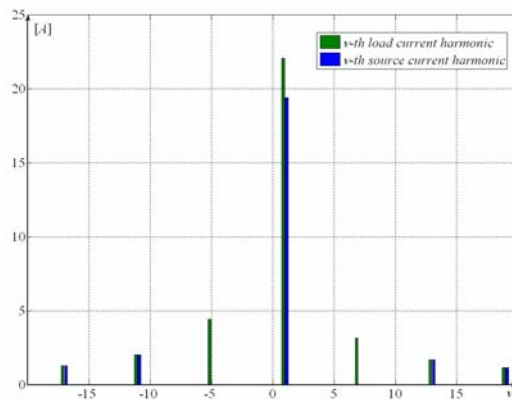
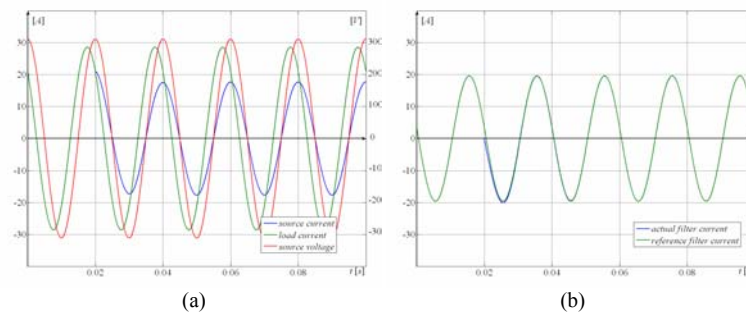


Fig.4.4. Harmonic analysis of load and source currents

Same results of this simulation are shown in figs.4.5. As fig.4.5a shows, the phase angle between the voltage and the line current is nil when the compensation algorithm is running. In fig.4.5d the inverter control functions $\zeta(t)$ and $\eta(t)$ are depicted. These present the 2nd harmonic, as fixed by eqs. (4.13) and (4.14), due to the interaction between the direct and inverse component of the first harmonic. Finally, although the load currents are unbalanced, figs. 4.5e and 4.5f show that the active filter, driven by the suggested control technique, is able to balance very well the line currents after only one period of the fundamental frequency.

Tab.4.III. Parameters of unbalanced passive load

$r_{L,1}$ [Ω]	$l_{L,1}$ [mH]	$r_{L,2}$ [Ω]	$l_{L,2}$ [mH]	$r_{L,3}$ [Ω]	$l_{L,3}$ [mH]
8.1	23.3	13.2	3.7	17.7	66.0



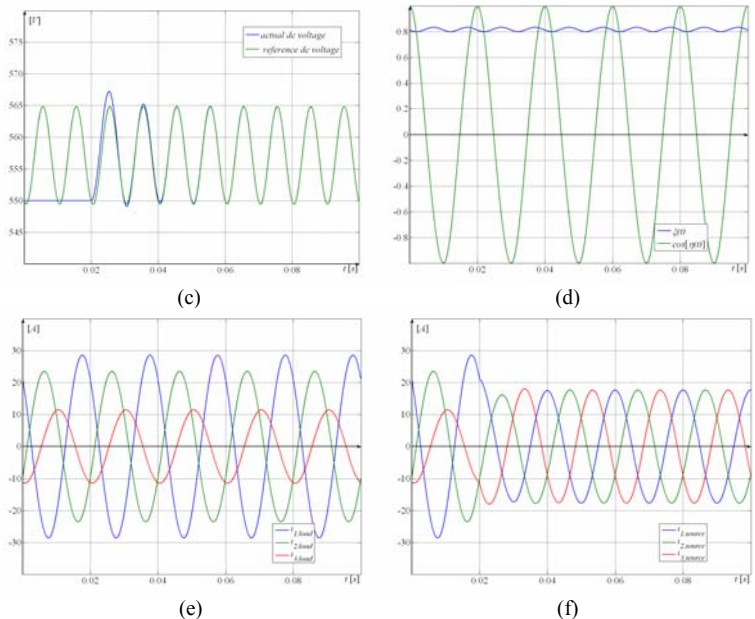


Fig.4.5. Digital simulation of load balancing using the suggested algorithm

IV.4. CONCLUSIONS

The chapter has shown how shunt active filters, used for current harmonic compensation, can be driven by inverse feeding algorithms simply expressed by means of analytical equations. This opportunity is offered by results obtained in the chapter II. These results are related to the analytical resolution of non linear differential equations that depict the dynamic behaviour of active filters. The suggested analytical procedure for the shunt active filter control appears to be very useful in practice, because it implies very simple control techniques and it is, besides, capable of giving rise to very accurate current harmonic compensation. The features of the suggested procedure are highlighted in this chapter by means of digital simulations, which fully validate that ones theoretically expected.

V

VALIDATION OF THE MATHEMATICAL MODEL: EXPERIMENTAL RESULTS

V.1. INTRODUCTION

The study of the behaviour of a physical system can be carried out by two different ways. A first type of approach makes use extensively of experimental tests and consists on the interpretation of the results with theoretical justifications. The second type of approach makes use of the mathematical models of physical systems and consists on the determination of a set of algebraic and/or differential equations whose resolution gives the unknown quantities of the system. This second approach is more useful than the previous one because the solution can be obtained for every values of inner parameters and for every inputs of the system. Since the evaluation of unknown quantities is obtained theoretically, a preliminary experimental validation of the mathematical model is required. The system is forced with known testing inputs and the unknown quantities are measured and stored into a database. If the accord between the solution theoretically obtained and the waveforms experimentally acquired is good, the mathematical model is validated and can be successfully used for the evaluation of the same solution in different operating conditions. In addition, the deviation between the theoretical and experimental solutions gives the approximation order of the model.

In this chapter, a comparison between the waveforms obtained by experimental tests and those evaluated by the analytical solution is presented. This has been made for different values of inner filter parameters and inverter output phase displacement. In addition, the dependence of filter performances on the values of passive elements has been illustrated and experimentally validated.

V.2. THE TEST BENCH

The test bench used for the validation of the mathematical model is represented in fig.5.1.

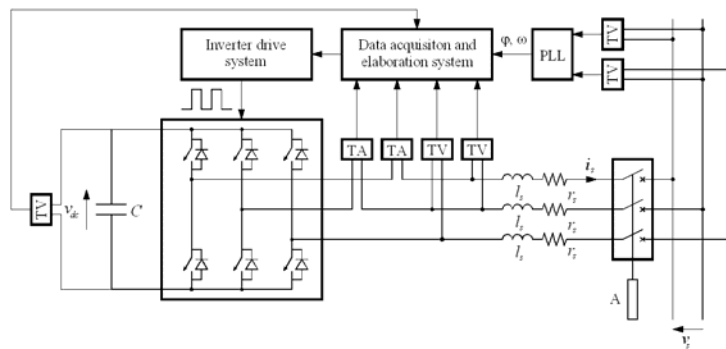


Fig.5.1. The test bench used for the experimental tests

The active filter has been connected in the Point of Common Coupling (PCC) to the three-phase distribution power network, whose ratings are a voltage of 380 V rms and a frequency of 50 Hz. A breaker between the filter and

the network allows the switch on and switch of the active filter and has also the function of protection against the short circuits. A picture of the PCC is shown in fig.5.2.

Fig.5.3 shows a picture of the passive filter connected to a leg of the inverter. This is a series of a shell-type inductor of 25 mH and a resistor adjustable from 0 to 101 Ω . Adjusting the value of the resistance it is possible to test the influence of inner parameters on the system behaviour.

The three-phase inverter is a voltage-source type with IGBT power switches. Fig.5.4 is a picture of the inverter and Tab.5.I summarises its main ratings. In fig.5.4 it is possible to see also the series of two capacitors on the dc-link side, each one having a capacitance of 3.3 mF.

The processor that has been used is the TMS320C30 of Texas Instruments with a clock frequency of 40 MHz. Although this type of processors can not anymore be considered as a state of the art DSP, its performance is still powerful enough for real-time machine control. In Tab.5.II its characteristics are shown. Its cycle time is equal to 50 ns and, in comparison with its successor, the TMS320C40, this cycle time is 10 ns slower. The most interesting feature of this processor is its two external data-buses. One bus (primary) is dedicated for fast I/O-control of the memory, which is located near the processor. The expansion bus (secondary) can be used for the communication with the peripherals and is therefore directly connected to the backplane. In order to avoid problems, the frequency on the expansion bus is set much lower than the internal clock frequency (40 MHz). The desired PWM output voltage can be obtained programming the DSP code by means of a software written in C environment.

The DSP is embedded in a backplane which contains inside other cards for the data acquisition and the data post-processing. The inverter command system, whose picture is shown in fig.5.5, is flexible because

Tab.5.I – Ratings of inverter used for experimental tests

Power [kVA]	Voltage [V]	Current [A]	Switching frequency [kHz]
22	380	40	10

Tab.5.II. - The characteristics of the TMS320C30-40MHz

Frequency [MHz]	40
MIPS	20
MFLOPS	40
Cycle Time [ns]	50
Data/Program Memory [Words]	16M
RAM [Words]	2k
ROM [Words]	4k
Cache	64
DMA	1
Timers	2
Serial ports	2
Parallel ports	16M x 32
Boot Loader Available	NO

there is a card for the 8 analogue inputs and the Analogue to Digital Conversion (ADC), a card for the 8 analogue outputs and the Digital to Analogue Conversion (DAC), a PWM card with both space vector and hysteretic modulation. These cards can be eventually replaced if for example a different number of analogue input is needed, or another pulse width modulation technique is required.

The DSP is connected to a personal computer, shown in fig.5.6, which is the core of the signal post-processing and the place where the data measured are store. Using the program language C, it is possible to program easily the DSP memory directly via PC.

The analogue signals are picked-up from the field by means of Hall-type current transducers (TA) and voltage transducers (TV). These transducers convert the power signals to voltage signals in the range $-10\text{ V} / 10\text{ V}$, that the ADCs can read and convert in digital form by means of digital converters of Burr-Brown. These 12 bit converters are characterised by a fast and parallel conversion. Each analogue input signal is converted within $2.7\ \mu\text{s}$. The conversion is initiated by a timer of the DSP, which is equal to the sample time of the control. During the conversion, the busy signals of the converters is active. A Printed Circuit Board (PCB) is designed with four AD-converters, which are located from a specific base-address. This base-address can be changed with the help of jumpers. When the four conversions are finished, i.e. every busy signal has become inactive, an interrupt is generated. After this interrupt the DSP starts the calculation once the measurements are available. If more AD-cards are applied in the system, the interrupt generation on the other cards has to be disabled, since more than one interrupt generates a conflict. In the main program the converted variables of the card, which has generated the interrupt, are read first. After that, it is safe to read the converted variables from the other Analogue to Digital converter cards. In order to prevent the aliasing effect, the AD-converters are equipped with a filter module. This module consists of 4 second order Butterworth low-pass filters with a cut-off frequency of 2.5 kHz and is placed on the PCB of the AD converters

The analogue outputs, given by DAC converters, are also in the range $-10\text{ V} / 10\text{ V}$ and can be sent to a digital scope in order to a fast visualisation of the quantities of interest. The converter that has been used is from Analogue

Devices and it is 12 bit wide and is mounted on a PCB, which contains four analogue outputs.



Fig.5.2. Three-phase supplying network

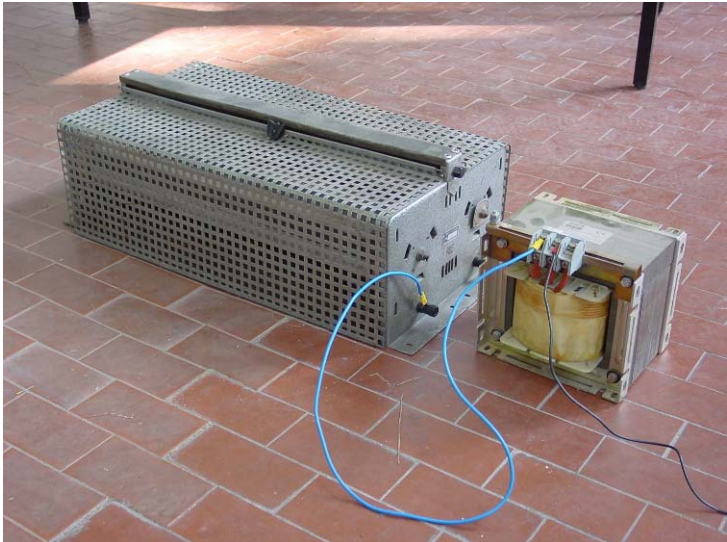


Fig.5.3. Passive filter made by the series of an adjustable resistor and a 25 mH inductor

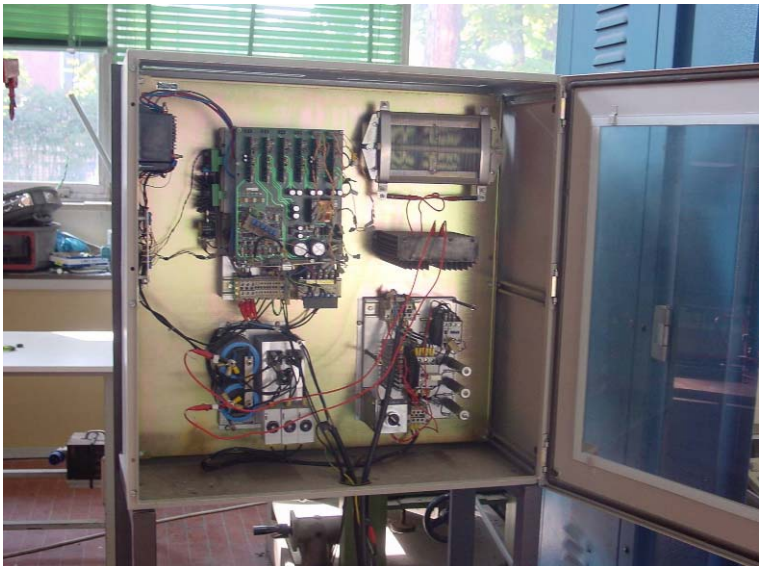


Fig.5.4. 22 kVA IGBT-based inverter VSI

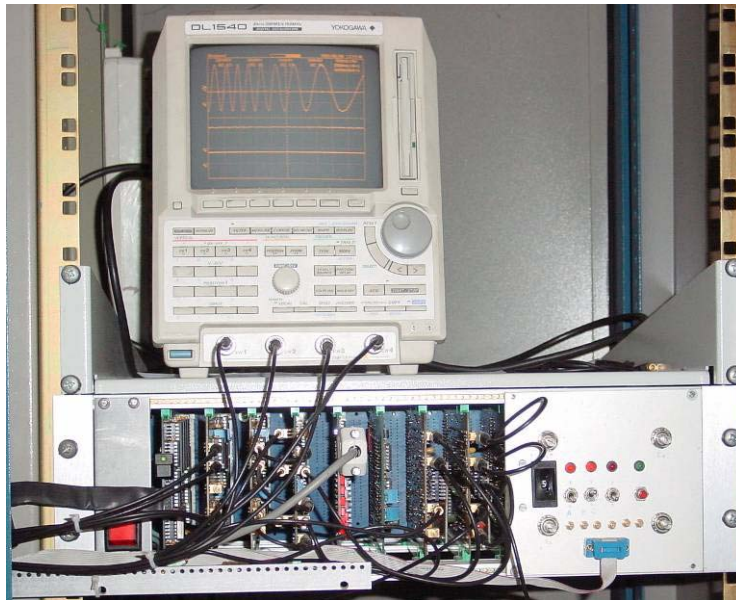


Fig.5.5. DSP-based inverter command system



Fig.5.6. Data acquisition and elaboration system

The active filter is connected to an active power network. For this reason the fundamental frequency of the inverter output voltage has to be the same of the network frequency, which is not always constant and equal to 50 Hz. Moreover, it is necessary to know also the phase displacement of the network voltage in order to apply the inverter voltage with the correct phase shift. An algorithm capable of detecting both the frequency and the phase displacement of network voltage is therefore needed. Such an algorithm has been implemented making use of a Phase-Locked Loop algorithm (PLL). The PLL technique has been used commonly for tracking and synthesising the phase and frequency information in electrical systems [15, 16]. In the area of power electronics, the PLL technique has been adopted in the speed control of electric motors [17, 18]. This is also available for synchronising the network voltages and the controlled currents or voltages in interface operations towards network of power electronic systems.

The block diagram of the three phase PLL system is represented in Fig.5.7. In this system, the three phase network voltages can be represented using the space vector representation in the stationary frame:

$$\mathbf{v}_s^s = \frac{2}{3} \left(v_{s1} + v_{s2} e^{j\frac{2\pi}{3}} + v_{s3} e^{j\frac{4\pi}{3}} \right). \quad (5.1)$$

Under the assumption of the balanced network voltage, (5.1) can be expressed as:

$$\mathbf{v}_s^s = \frac{2}{3} V_s \left[\cos\varphi + \cos\left(\varphi - \frac{2\pi}{3}\right) e^{j\frac{2\pi}{3}} + \cos\left(\varphi - \frac{4\pi}{3}\right) e^{j\frac{4\pi}{3}} \right] = V_s e^{j\varphi}.$$

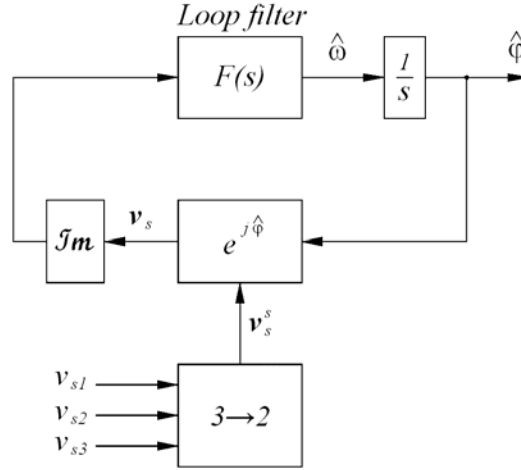


Fig.5.7. Block diagram of three phase PLL system

This equation can be rewritten in the synchronous reference frame using the PLL output $\hat{\phi}$ as:

$$\mathbf{v}_s = \mathbf{v}_s^s e^{-j\hat{\phi}} = V_s e^{j(\varphi - \hat{\phi})}.$$

The projection of this complex equation onto the imaginary axis yields:

$$v_s^I = V_s \sin(\varphi - \hat{\phi}) = V_s \sin\delta = e$$

where $\delta = \varphi - \hat{\phi}$. The angular frequency of the PLL system can be represented as:

$$\hat{\omega} = \frac{d\hat{\phi}}{dt} = K_f e \quad (5.2)$$

where K_f denotes the gain of the loop filter. If the phase difference δ is very small, eq. (5.2) can be rewritten approximately as:

$$e \cong V_s \delta.$$

Hence, the PLL frequency $\hat{\omega}$ and phase $\hat{\phi}$ are able to track respectively the network frequency ω and phase angle φ by a proper design of the loop filter.

The linear model of the three phase PLL system can be described as shown in Fig.5.7. The transfer function of the closed loop system can be represented as:

$$H(s) = \frac{\hat{\Phi}(s)}{\Phi(s)} = \frac{F(s)V_s}{s + F(s)V_s}$$

where $\Phi(s)$ and $\hat{\Phi}(s)$ denote the Laplace transform of φ and $\hat{\phi}$, respectively. There are different methods in designing the loop filter. The second order loop is commonly used as a good trade-off of the filter performance and

system stability [15]. The proportional-integral (PI) type filter for the second order loop can be given as:

$$F(s) = K_f \frac{1 + s\tau}{s\tau}$$

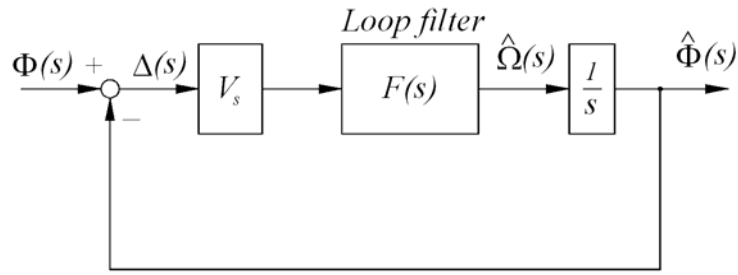


Fig.5.8. Linear model of three phase PLL system

where K_f and τ denote the gains of the PI type filter. The transfer functions of the closed loop system are rewritten in the general form of the second order loop as:

$$H(s) = \frac{2\zeta\omega_n s + \omega_n^2}{s^2 + 2\zeta\omega_n s + \omega_n^2}$$

where:

$$\omega_n = \sqrt{\frac{K_f V_s}{\tau}} ;$$

$$\zeta = \frac{K_f V_s}{2\omega_n} = \frac{\sqrt{\tau K_f V_s}}{2} .$$

The closed loop bandwidth is chosen equal to 100 Hz, i.e. $\omega_n = 628$ rad/s, where the damping ratio is chosen as $\zeta = 0.707$ and the peak of the network voltage V_s is 311 V. Under these conditions, the gains of the loop filter are given as $K_f = 2.85$, and $\tau = 0.002247$, respectively. The chosen values are a compromise between a fast dynamic response, given by a larger bandwidth, and a greater effectiveness to reduce the output ripple, given by the low pass filtering effects.

V.3. EXPERIMENTAL RESULTS WITHOUT INDUCTANCES

The validation of the mathematical model has been carried out making a comparison between the waveforms experimentally measured and those evaluated by the analytical solution. The first tests have been

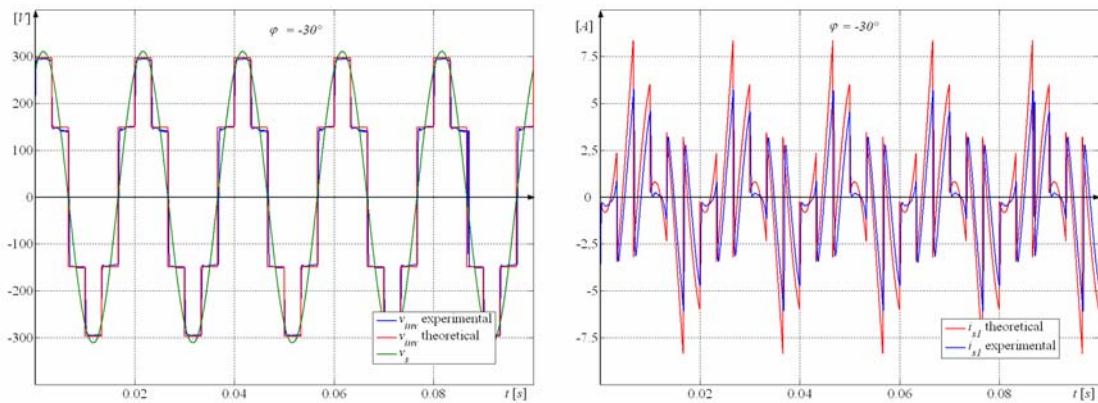


Fig.5.9. Comparison between experimental and theoretical voltages (a) and currents (b) with $\varphi = -30^\circ$, $r_s = 7.5 \Omega$.

performed without the filter inductances, with a resistance of 7.5 Ω and a phase angle $\varphi = -30^\circ$. The quantities

measured have been the output inverter voltage, the source voltage and the current in a leg of the active filter. The results have been reported in the figs.5.9. The same test has been made with a different phase displacement $\varphi = 0^\circ$ and the comparison is shown in figs.5. 10.

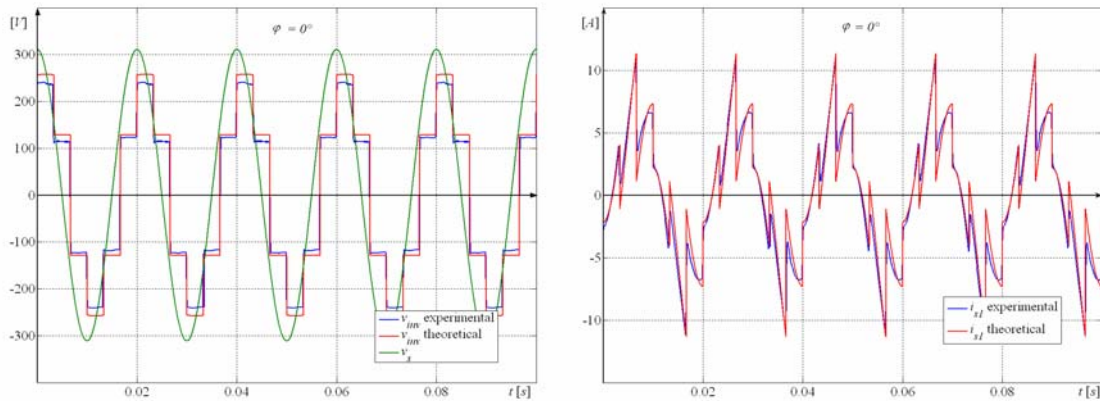


Fig.5.10. Comparison between experimental and theoretical voltages (a) and currents (b) with $\varphi = 0^\circ$, $r_s = 7.5 \Omega$

The analysis of figs.5.9 and 5.10 points out that the waveforms analytically evaluated are in a very good agreement with those measured from the field. The actual current has the same discontinuities foreseen by the suggested solution. The difference between the amplitude of the theoretical and experimental square wave inverter voltages involves also a light disagreement of the peak value of the current. This error, perceptible when $\varphi = -30^\circ$, is in practice insignificant when $\varphi = 0^\circ$.

V.4. EXPERIMENTAL RESULTS WITH INDUCTANCES

The same comparison between the waveforms experimentally measured and those evaluated by the analytical solution has been performed for the filter connected to the network by means of a series of an inductor and a resistor. The results have been reported in the next fig.5.11.

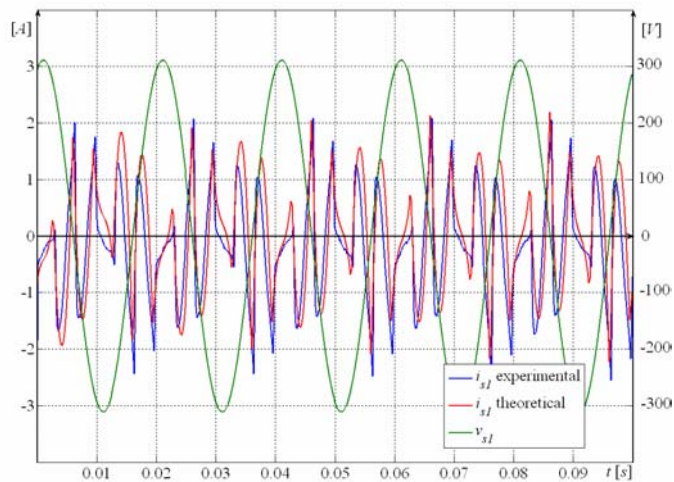


Fig.5.11. Comparison between experimental and theoretical currents with $\varphi = -30^\circ$, $r_s = 10 \Omega$ and $l_s = 25 \text{ mH}$

The comparison between the current waveforms denotes a good tracking of the analytical solution. The differences respect to the experimental waveforms can be attributed to the saturation of the inductance that the mathematical model neglects.

Another test with different parameter values and phase displacement has been executed and the results have been represented in fig.5.12. The results highlight that for a smaller inductance the agreement between the

experimental waveform and the analytical solution is better.

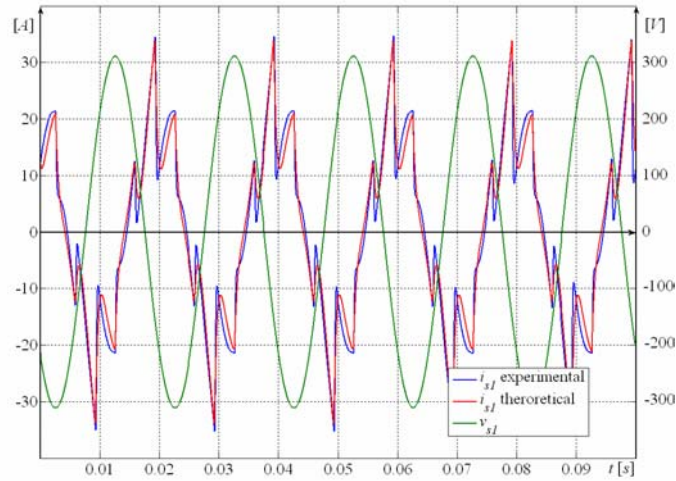


Fig.5.12. Comparison between experimental and theoretical currents with $\phi = 0^\circ$, $r_s = 7.5 \Omega$ and $l_s = 2.5 \text{ mH}$

Another aspect that the validation of the mathematical model requires is the analysis of active filter performances respect to some goals. The quantities of interest has been the rms current supplied to the network, the reactive power compensated and the power losses of the passive r-l filter. A preliminary analysis of the dependence of these performance markers on the passive filter parameters has been needed using the analytical solution illustrated in the chapter II. The diagrams are reported as a function of the phase displacement ϕ between network voltage and inverter output voltage and are parametric respect to the resistance, the inductance and the capacitance. These diagrams are shown respectively in figs.5.13, 5.14 and 5.15.

The compared analysis of figs.5.13 and 5.14 highlights that the

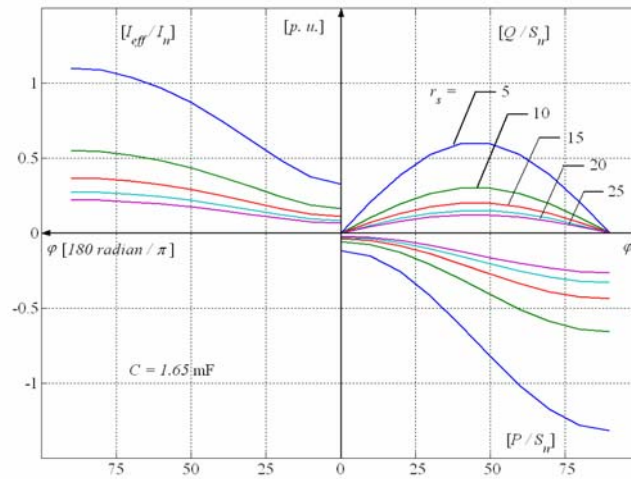


Fig.5.13. Reactive power compensated, power losses and rms current with different resistances

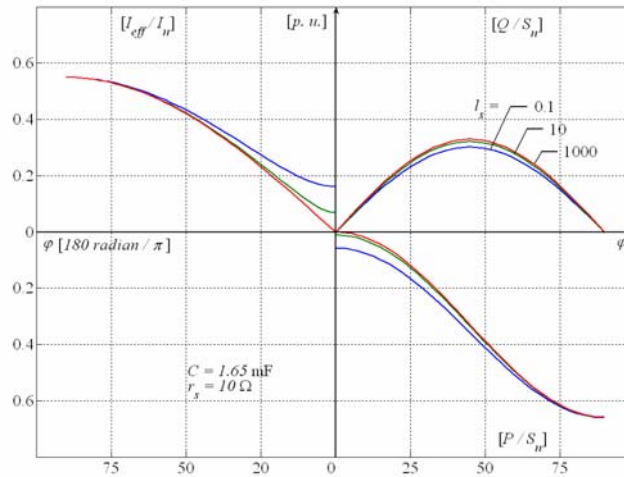


Fig.5.14. Reactive power compensated, power losses and rms current with different inductances

resistance and the inductance of the filter play a different role for the filter behaviour. When φ is near to 0° , i.e. the network voltage and the first harmonic of the inverter voltage are in phase, the first harmonic of the current is very small and comparable with the higher harmonics. Since the inductance reduces the higher harmonics, the rms current is affected by the inductance value more than by the resistance. Conversely when φ is greater than 60° , the fundamental harmonic is much more greater than the higher harmonics and therefore the value of the inductance slightly affects the rms current. The fundamental harmonic is in practice dependent only on the filter resistance and increases when the resistance decreases.

The dependence of the filter performances on the capacitance of dc-side capacitor has been also investigated. As fig.5.15 points out, the behaviour of the filter in terms of rms current, reactive power compensated and power losses in independent on the capacitance within

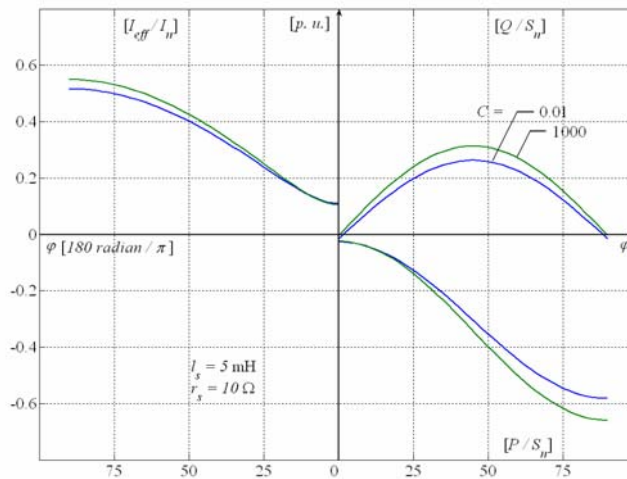


Fig.5.15. Reactive power compensated, power losses and rms current with different capacitances

a very large range of values (0.01 mF up to 1 F). It has been noted that the capacitance strongly affects the dc voltage ripple. However, this ripple can be considered negligible if the capacitance is at least 1 mF .

The experimental verification of the diagrams presented and discussed before has been finally carried out. This is shown in fig.5.16 in the case of different filter resistances where the cross are representative of measured points.

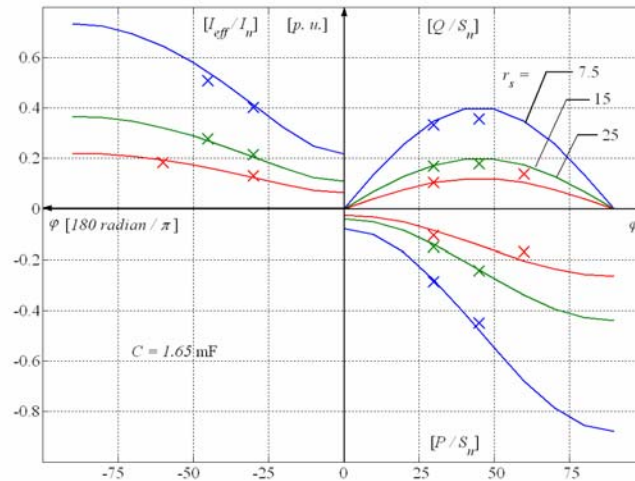


Fig.5.16. Experimental validation of previous diagrams

V.5. CONCLUSIONS

The study of physical systems can be successfully carried out by means of mathematical models. Once the mathematical models have been theoretically solved, the experimental validation is needed in order to verify if the models depict the behaviour of the physical systems they represent. The verification of the effectiveness of the mathematical procedure suggested in the previous chapters has been performed by means of experimental measurements of the voltage and current waveforms of a shunt active filter connected to the power network. The agreement between experimental and theoretical results fully validates the mathematical procedure suggested and allows the analysis of filter performances with different parameter values of passive elements and different phase displacements of inverter output voltage.

REFERENCES

- [1] Bird, B. M.; Marsh, J. F.; McLellan P. R.: "Harmonic reduction in multiple converters by triple-frequency current injection", IEE Proceedings (1969), vol. 116, n. 10, pp. 1730-1734.
- [2] Sasaki, H.; Machida T.: "A new method to eliminate ac harmonic currents by magnetic compensation-consideration on basic design", IEEE Trans. Power Appl. Syst. (1971), vol. 90, n. 5, pp. 2009-2019.
- [3] Ametani, A.: "Harmonic reduction in thyristor converters by harmonic current injection," IEEE Trans. Power Appl. Syst. (1976), vol. 95, n. 2, pp. 441-449.
- [4] Gyugyi, L.; Strycula, E. C.: "Active ac power filters", Proceedings of the 1976 IEEE/IAS Annual Meeting (1976), pp. 529-535.
- [5] Mohan, N.; Peterson, H. A.; Long, W. F.; Dreifuerst, G. R.; Vithaythil, J. J.: "Active filters for ac harmonic suppression", Proceedings of the 1977 IEEE/PES Winter Meeting (1977), A77026-8.
- [6] Uceda, J.; Aldana, F.; Martinez, P.: "Active filters for static power converters", IEE Proceedings (1983), vol. 130, pt. B, n. 5, pp. 347-354.
- [7] Kawahira, H.; Nakamura, T.; Nakazawa, S.; Nomura, M.: "Active power filters", Proceedings of the 1983 International Power Electronics Conference (1983), Tokyo, Japan, pp. 981-992.
- [8] Akagi, H.; Kanazawa, Y.; Nabae, A.: "Generalized theory of the instantaneous reactive power in three-phase circuits", Proceedings of the 1983 International Power Electronics Conference (1983), Tokyo, Japan, pp. 1375-1386.
- [9] Akagi, H.; Kanazawa, Y.; Nabae, A.: "Instantaneous reactive power compensators comprising switching devices without energy storage components", IEEE Trans. Ind. Appl. (1984), vol. 20, n. 3, pp. 625-630.
- [10] Akagi, H.; Nabae, A.; Atoh, S.: "Control strategy of active power filters using multiple voltage-source PWM converters", IEEE Trans. Ind. Appl. (1986), vol. 22, n. 3, pp. 460-465.
- [11] Jury, E. I.: "Theory and application of the z-transform method", John Wiley and Sons, New York (1964).
- [12] Mohan, N.; Undeland, T. M.; Robbins, W.P.: "Power Electronics", pp. 750-767. John Wiley & Sons, New York (2003).
- [13] Pagano, E.; Perfetto, A.: "Costruzioni elettromeccaniche", Edizioni Massimo, Napoli (1979).
- [14] Akagi, H.; Nabae, A.: "The p-q power theory in three-phase systems under non-sinusoidal conditions", ETEP (1993), vol. 3, issue 1, pp. 27-31.
- [15] Gardner, F. M.: "Phase-lock Techniques", John Wiley and Sons, New York (1979).
- [16] Razavi, B.: "Monolithic Phase-Locked Loop and Clock Recovery Circuit" IEEE Press, New York (1996).
- [17] Blasko, V.; Moreira, J. C.; Lipo, T. A.: "A new field oriented controller utilizing spatial position measurement of rotor end ring current," Proceedings of the Power Electronics Specialist Conference (1989), pp. 295-299.
- [18] Nozari, F.; Mezs, P. A.; Julian, A. L.; Sun, C.; Lipo, T. A.: "Sensorless synchronous motor drive for use on commercial transport airplanes", IEEE Trans. Ind. Applicat. (1995), vol. 31, pp. 850-859.
- [19] Das, J.C.: "Passive Filters - Potentialities and Limitations", IEEE Trans. Industry Applications (2004), vol. 40, issue 1, pp 232-241.

- [20] Czarnecki, L.S.: "New power theory of the 3-phase non-linear asymmetrical circuits supplied from non sinusoidal voltage sources", IEEE International Symposium on Circuits and Systems (1988), vol. 2, pp. 1627-1630.
- [21] Czarnecki, L.S.: "Orthogonal decomposition of the currents in a 3-phase nonlinear asymmetrical circuit with a non sinusoidal voltage source", IEEE Trans. Instrumentation and Measurement (1988), vol. 37, issue 1, pp. 30-34.
- [22] Czarnecki, L.S.: "Minimisation of unbalanced and reactive currents in three-phase asymmetrical circuits with non sinusoidal voltage", IEE Proceedings Electric Power Applications (1992), vol. 139, issue 4, pp. 347-354.
- [23] Po-Tai Cheng; Bhattacharya, S.; Divan, D.: "Experimental verification of dominant harmonic active filter (DHAF) for high power applications", Proceedings of the Industry Applications Conference (1998), vol. 2, pp. 1400-1407.
- [24] Rossetto, L.; Tenti, P.: "Using AC-fed PWM converters as instantaneous reactive power compensators", Proceedings of the Power Electronics Specialists Conference (1990), pp. 855-861.
- [25] Nishijima, T.; Tanaka, M.; Imayanagita, A.; Chen, Y.-F.; Fujikawa, K.; Kobayashi, H.: "Direct instantaneous harmonic distortion minimization control for three phase sinusoidal current converter", Proceedings of the Power Electronics Specialists Conference (1998), vol. 1, pp. 510-516.
- [26] Malesani, L.; Mattavelli, P.; Buso, S.: "Robust dead-beat current control for PWM rectifiers and active filters", Proceedings of the Industry Applications Conference (1998), vol. 2, pp. 1377-1384.
- [27] Dong-Chofson Lee; Ki-Do Lee; G-Myoung Lee: "Voltage control of PWM converters using feedback linearization", Proceedings of the Industry Applications Conference (1998), vol. 2, pp. 1491-1496.
- [28] Bhattacharya, S.; Divan, D.: "Design and implementation of a hybrid series active filter system", Proceedings of the Power Electronics Specialists Conference(1995), vol. 1, pp. 189-195.
- [29] Nastran, J.; Cajhen, R.; Seliger, M.; Jereb, P.: "Active power filter for nonlinear AC loads", IEEE Trans. Power Electronics (1994), vol. 9, issue 1, pp. 92-96.
- [30] Po-Tai Cheng; Bhattacharya, S.; Divan, D.D.: "Line harmonics reduction in high-power systems using square-wave inverters-based dominant harmonic active filter", IEEE Trans. Power Electronics (1999), vol. 14, issue 2, pp. 265-272.
- [31] Po-Tai Cheng; Bhattacharya, S.; Divan, D.M.: "Control of square-wave inverters in high-power hybrid active filter systems", IEEE Trans. Industry Applications (1998), vol. 34, issue 3, pp. 458-472.
- [32] Aliouane, K.; Saadate, S.; Davat, C.: "Analytical study and numerical simulation of the static and dynamic performances of combined shunt passive and series active filters", Proceedings of the Fifth International Conference on Power Electronics and Variable-Speed Drives (1994), pp. 147-151.
- [33] Chen, Z.; Blaabjerg, F.; Pedersen, J.K.: "A study of parallel operations of active and passive filters", Proceedings of the Power Electronics Specialists Conference (2002), vol. 2, pp. 1021-1026.
- [34] Lijun Chen; von Jouanne, A.: "A comparison and assessment of hybrid filter topologies and control algorithms", Proceedings of the Power Electronics Specialists Conference (2001), vol. 2, pp. 565-570.
- [35] Krah, J.-O.; Holtz, J.: "Total compensation of line-side switching harmonics in converter-fed AC locomotives", Proceedings of the Industry Applications Society Annual Meeting (1994), vol. 2, pp. 913-920.
- [36] Xu, J.H.; Saadate, S.; Davat, B.: "Compensation of AC-DC converter input current harmonics using a voltage-source active power filter", Proceedings of the Fifth European Conference on Power Electronics and Applications (1993), vol. 8, pp. 233-238.
- [37] Chen Guozhu; Zhengyu Lu; Qian Zhaoming: "The design and implement of series hybrid active power filter

- for variable nonlinear loads”, Proceedings of the Power Electronics and Motion Control Conference (2000), vol. 3, pp. 1041-1044.
- [38] Terbobri, G.G.; Saidon, M.F.; Khanniche, M.S.: “Trends of real time controlled active power filters”, Proceedings of the IEE Conference (2000), publ. n. 475, pp. 410-415.
- [39] Bocchetti, G.; Carpita, M.; Giannini, G.; Tenconi, S.: “Line filter for high power inverter locomotive using active circuit for harmonic reduction”, Proceedings of the Fifth European Conference on Power Electronics and Applications (1993), vol. 8, pp. 267-271.
- [40] Moran, L.; Diaz, M.; Higuera, V.; Wallace, R.; Dixon, J.: “A three-phase active power filter operating with fixed switching frequency for reactive power and current harmonic compensation”, Proceedings of the International Conference on Industrial Electronics, Control, Instrumentation, and Automation (1992), vol. 1, pp. 362-367.
- [41] Ali, S.M.; Kazmierkowski, M.P.: “Current regulation of four-leg PWM/VSI”, Proceedings of the Industrial Electronics Society (1998), vol. 3, pp. 1853-1858.
- [42] Gun-Woo Moon; Suk-Ho Yoon: “Predictive current control of distribution static condenser (D-STATCON) for reactive power compensation in flexible AC transmission system (FACTS)”, Proceedings of the Power Electronics Specialists Conference (1998), vol. 1, pp. 816-822.
- [43] Aburto, V.; Schneider, M.; Moran, L.; Dixon, J.: “An active power filter implemented with a three-level NPC voltage-source inverter”, Proceedings of the Power Electronics Specialists Conference(1997), vol. 2, pp. 1121-1126.
- [44] Dastfan, A.; Platt, D.; Gosbell, V.J.: “Design and implementation of a new three-phase four-wire active power filter with minimum components”, Proceedings of the Industry Applications Conference (1998), vol. 2, pp. 1369-1376.
- [45] Verdelho, P.: “Space vector based current controller in $\alpha\beta 0$ coordinate system for the PWM voltage converter connected to the AC mains”, Proceedings of the Power Electronics Specialists Conference (1997), vol. 2, pp. 1115-1120.
- [46] Bonifacio, G.; Lo Schiavo, A.; Marino, P.; Testa, A.: “A new high performance shunt active filter based on digital control”, Proceedings of the Power Engineering Society Winter Meeting (2000), vol. 4, pp. 2961-2966.
- [47] Valouch, V.: “Active filter control methods based on different power theories”, IEEE Trans. Industrial Electronics (1999), vol. 2, pp. 521-526.
- [48] Lin, C.E.; Tsai, M.T.; Shiao, Y.S.; Huang, C.L.: “An active filter for reactive and harmonic compensation using voltage source inverter”, Proceedings of the International Conference on Advances in Power System Control, Operation and Management (1991), vol. 2, pp. 588-593.